

Accurate identification of moving vehicle loads on beam-like bridge structures integrating novel PCA-based dictionary with grouping and weighting strategy

Bohao Xu, Zhilong Hou, Yuhua Chen, Ling Yu*

MOE Key Laboratory of Disaster Forecast and Control in Engineering, School of Mechanics and Construction Engineering, Jinan University, Guangzhou 510632, China

ARTICLE INFO

Keywords:

Vehicle-bridge interaction
Moving load identification (MLI)
Principal component analysis (PCA)
Group Lasso
Alternating direction method (ADM)

ABSTRACT

Most moving load identification (MLI) methods incorporate the dictionary theory as a regularization technique to address the ill-posedness of the problem. However, the selection of atoms in the dictionary often inadequately represents the actual vehicle loads in existing methods, and the prior information from these atoms is disregarded in the subsequent MLI computations. Therefore, a novel MLI framework is proposed for beam-like bridge structures based on a novel dictionary derived from principal component analysis (PCA) and newly grouping and weighting strategy in this study. At first, a vehicle-bridge coupling system (VBCS) is established to obtain the interaction forces between the moving vehicles and bridge deck. The system matrices between the interaction forces and structural responses are derived in the time domain. The PCA technique is then employed to extract information from these interaction forces and to subsequently construct a PCA-based dictionary. Based on the eigenvalues of each principal component in the dictionary, a weighted group sparse model, incorporating the newly grouping and weighting strategy, is defined to obtain the coefficients of each atom. The solution to this model is obtained using the alternating direction method (ADM). Finally, the proposed method is validated in numerical simulations comparing with some existing methods. The effects of noise levels, road surface roughness, number of training data, response combinations and the tolerances in ADM were also studied. Similarity law for the VBCS is conducted in experimental verifications to construct the PCA-based dictionary, allowing for a reasonable identification of gross vehicle weights. The results indicate that the MLI accuracy has been enhanced by the proposed method, and the similarity law employed in experiments is reasonable. Setting the tolerance in ADM as $\epsilon = 1 \times 10^{-5}$ can lead to a higher accuracy and reduce the computation cost in both numerical simulations and experimental verifications.

1. Introduction

Moving vehicle loads are the primary live loads on bridges and provide crucial information for structural health monitoring, bridge design and safety assessments [1]. They are usually deemed as two parts such as the static and dynamic components. Most studies focus on the identification of static load for the purpose of monitoring vehicle weight and averting instances of overweight [2,3]. However, the dynamic components of moving vehicle loads, which may result in a 2–4 times

increase in road surface damage compared to that caused by the static component, are one of challenging tasks to extract directly in comparison with the static component [4]. When the vehicles are moving across a bridge structure, the dynamic components are not only contingent upon the intrinsic parameters of the vehicles themselves but also correlated with road surface roughness (RSR) [5]. Various indirect methods have been developed to address this issue by utilizing structural responses associated with the vehicle and structural characteristics of bridges [6]. There are lots of ways to establish the relationship between

Acronyms and abbreviations: ADM, alternating direction method; ADMM, alternating direction method of multipliers; BOMP, batch orthogonal matching pursuit; CR, cumulative ratio; Lasso, least absolute shrinkage and selection operator; MFI, moving force identification; MLI, moving load identification; MP, matching pursuit; MVL, moving vehicle load; NRAMP, novel regularized adaptive matching pursuit; OMP, orthogonal matching pursuit; PC, principal component; PCA, principal component analysis; PCS, principal component space; RPE, relative percentage error; RSR, road surface roughness; SRP, sparse recovery problem; TDM, time domain method; VBCS, vehicle-bridge coupling system.

* Corresponding author.

E-mail address: lyu1997@163.com (L. Yu).

vehicle and structural responses such as time domain method (TDM) [7], finite element method, updated static component method [8] and so on. Compared to the forward problem, the moving vehicle load identification as an inverse problem needs a greater level of analytical rigor due to its higher susceptibility to singularities and other indeterminacies [9]. To tackle the ill-posedness in the inverse problem, a number of methods such as the regularization, deep learning, and Bayesian methods [10–13], have been proposed and great progress made. Especially for the regularization methods, they have been paid attention extensively.

Regularization methods, commonly employed to address the inherent challenges of inverse problems, have found widespread application in the realm of moving force identification (MFI). The classical Tikhonov method has been applied in MFI by Law and Zhu under the assumption that the moving force is a dense solution [14,15]. According to the inverse problem in MFI, represented as a large linear system, a preconditioned least square QR-factorization regularization method is proposed by Chen *et al.* to solve it [16]. Pan *et al.* [17] introduced dictionary theory to MFI, transforming the original problem into a sparse recovery problem (SRP). The dictionary consists of trigonometric functions and rectangular functions, which are called basis functions or atoms of the dictionary. With the utilization of this dictionary, various methods, such as the least absolute shrinkage and selection operator (Lasso), have been introduced as the primary technologies to address SRP. The estimated solution by the Lasso is to minimize the residual of SRP by adding a constraint on the l_1 -norm of solution [18]. Liu *et al.* [19] proposed a reweighted l_1 -norm regularization method to solve SRP, and it has been applied into a five-span bridge to identify truck weights. Qiao *et al.* [20] proposed a primal-dual interior point method to identify impulse force which is also a SRP. Jiang *et al.* proposed a selection method of basis functions to solve SRP problem based on the type of loads [21]. These methods exhibit excellent robustness to noise and solve the ill-posedness to a certain extent. They indicated that the choice of regularization parameter plays a significant role in the final results. However, it is not fixed with changes in work conditions sometimes so that it should be rechosen in different cases.

To avoid this problem, the matching pursuit (MP) algorithm, which is used to find the most relevant basis function in the dictionary, has been introduced by some researchers. Liu *et al.* [22] used signal space compressive sampling MP algorithm to solve MFI based on compressing sensing and dictionary theory. Zhang *et al.* [23] proposed a novel method based on learning dictionary and double sparsity to solve MFI. The initial dictionary consists of trigonometric functions, and the orthogonal MP (OMP) algorithm is used in the SPR during the entire calculation process. Xu and Yu [24] proposed a novel regularized adaptive MP (NRAMP) algorithm to solve the unknown sparsity and ill-posedness with the introduction of MP algorithm. Therefore, the existing method based on MP algorithm can handle the SRP problem effectively. However, the prior information of each sparse atom has not been effectively utilized yet for further accuracy.

Based on the assumption that the solution to MFI can be regarded as a group within a time domain, the group sparse regularization has been incorporated in the force reconstruction. Qiao *et al.* [25] used an accelerated gradient descent method to solve the group sparse model by adding mixed l_{2-1} norm to the solution. With the dictionary consisting of trigonometric functions, Zhang *et al.* [26] introduced a modified orthogonal matching pursuit algorithm to solve the MFI. The influence of the number of groups is also considered in the simulations and experiments. Liu *et al.* [27] proposed an efficient alternating direction method of multipliers (ADMM) for addressing the challenge of overlapping group sparsity. They also explored the implications of group size on the identification process. Liang *et al.* [28] proposed an improved batch orthogonal matching pursuit (BOMP) algorithm with atom screening strategy to solve the SRP in the same dictionary. The results were great under the assumption that the moving force is composed of relatively dense frequency components in a small domain. However, the

weights of each group are not considered in their work, and the number of atoms in each group still need a further improvement according to the dictionary. Furthermore, the choice of the atom in dictionary should be chosen reasonably according to the real vehicle load. Even though the results based on the dictionary consisting of trigonometric functions were great in the preceding studies, the simulated moving forces are mainly composed of trigonometric functions that correspond to the atoms in the dictionary.

Principal component analysis (PCA), which is the most popular technique to analyze data, decomposes the data into components that capture the maximum variance, enabling the reconstruction of the data through a linear combination of these components. Due to this characteristic, the PCA technology has been widely used in structural health monitoring, image classification, face recognition and so on [29–32]. Inspired by the work in Ref [32], a novel dictionary called PCA-based dictionary is established by PCA. Unlike the existing work in Ref [30] by Prawin, where both the responses and input forces are transformed into principal component space (PCS), this study focuses more on transforming only the prior information of the moving vehicle loads into PCS. With this technology, the prior information of some vehicle models can be added into the dictionary so that the solution to the MFI is more accurate. Furthermore, the eigenvalues of each principal component (PC) can serve as a prior information for the atoms in dictionary theory, aiding in further calculations.

In this study, a new MLI framework is proposed for the beam-like bridge structures based on a novel principal component analysis (PCA)-based dictionary and a newly weighting and grouping strategy. At first, a vehicle-bridge coupling system (VBCS) with different road surface roughness (RSR) is established to present the vehicle-bridge interaction forces. Then the relationship between beam-like bridge responses and interaction forces are established in time domain. A novel dictionary is constructed by the principal component analysis (PCA) according to a half vehicle model under different RSR levels. Finally, the MLI problem is converted into a group sparse model by adding the weighted l_{2-1} norm. A newly grouping and weighting strategy is proposed according to the obtained PCA-based dictionary, and the final solution to the MLI problem is obtained by the alternating direction method (ADM).

The structure of this paper is organized as follows. In Section 2, the theoretical framework of the proposed method is proposed for the MLI problem in the beam-like bridge structures, in which a novel PCA-based dictionary and group sparse model using a newly grouping and weighting strategy are introduced. Some numerical simulations on moving vehicle load identification under different methods, road surface roughness, response combinations, noise levels and tolerances in ADM are carried out in Section 3. In Section 4, the feasibility of the proposed method is further assessed through experimental verifications conducted in laboratory. Finally, some conclusions are drawn in Section 5.

2. Theoretical framework

2.1. Motion equation for vehicle-bridge coupling system (VBCS)

As shown in Fig. 1, a simply supported beam bridge subjected to a vehicle, which is modeled as a half vehicle model, is taken to establish the VBCS. If the bridge is discretized into n beam elements, the beam finite element model can be established [33,34]:

$$\mathbf{M}_b \ddot{\mathbf{y}}_{br} + \mathbf{C}_b \dot{\mathbf{y}}_{br} + \mathbf{K}_b \mathbf{y}_{br} = \mathbf{H}_c \mathbf{P}, \quad (1)$$

where, \mathbf{M}_b , \mathbf{C}_b and \mathbf{K}_b are the mass, damping and stiffness matrices of the bridge, respectively. \mathbf{y}_{br} is nodal displacement of the bridge. \mathbf{H}_c is the global transfer matrix which transforms the interaction axle load into the equivalent nodal load, and it is established by:

$$\mathbf{H}_c = \begin{bmatrix} \mathbf{O} & \mathbf{O} & \cdots & \mathbf{O} & \mathbf{H}_1 & \cdots & \mathbf{O} \\ \mathbf{O} & \mathbf{O} & \cdots & \mathbf{H}_2 & \mathbf{O} & \cdots & \mathbf{O} \end{bmatrix}^T, \quad (2)$$

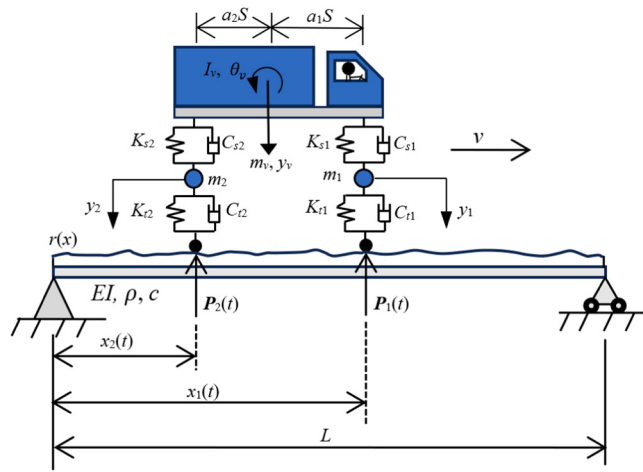


Fig. 1. Vehicle-bridge coupling system.

where, the \mathbf{H}_i is the Hermite shape function related to the i th vehicle axle load, \mathbf{O} is a matrix or vector composed of zero element.

With the Lagrange formulation, the equation of motion of half vehicle model can be obtained [33,35,36]:

$$\begin{bmatrix} \mathbf{M}_{v1} & \mathbf{O} \\ \mathbf{O} & \mathbf{M}_{v2} \end{bmatrix} \ddot{\mathbf{Y}} + \begin{bmatrix} \mathbf{C}_{v11} & \mathbf{C}_{v12} \\ \mathbf{C}_{v21} & \mathbf{C}_{v22} \end{bmatrix} \dot{\mathbf{Y}} + \begin{bmatrix} \mathbf{K}_{v11} & \mathbf{K}_{v12} \\ \mathbf{K}_{v21} & \mathbf{K}_{v22} \end{bmatrix} \mathbf{Y} = \begin{bmatrix} \mathbf{O} \\ \mathbf{M}_s \end{bmatrix} - \begin{bmatrix} \mathbf{P} \end{bmatrix}, \quad (3)$$

where, \mathbf{M}_{v1} , \mathbf{M}_{v2} , \mathbf{C}_{v11} , \mathbf{C}_{v12} , \mathbf{C}_{v21} , \mathbf{C}_{v22} , \mathbf{K}_{v11} , \mathbf{K}_{v12} , \mathbf{K}_{v21} and \mathbf{K}_{v22} are the mass, damping and stiffness sub-matrices of the vehicle, respectively. $\mathbf{Y} = [y_v \ \theta_v \ y_1 \ y_2]^T$ is the displacement vector of the vehicle. \mathbf{M}_s is composed of the static load of each vehicle axles. The more details of them are given in Appendix. \mathbf{P} is an interaction force vector between the bridge and each of vehicle axles:

$$\begin{aligned} \mathbf{P} = \begin{bmatrix} \mathbf{P}_1(t) \\ \mathbf{P}_2(t) \end{bmatrix} &= \begin{bmatrix} K_{t1}(y_1 - w(x_1(t), t) - r(x_1(t))) \\ K_{t2}(y_2 - w(x_2(t), t) - r(x_2(t))) \end{bmatrix} \\ &+ \begin{bmatrix} C_{t1}(y_1 - \dot{w}(x_1(t), t)) + (m_1 + a_2 m_v) g \\ C_{t2}(y_2 - \dot{w}(x_2(t), t)) + (m_2 + a_1 m_v) g \end{bmatrix}, \end{aligned} \quad (4)$$

where, $x_1(t)$ and $x_2(t)$ are the positions of the first and second axle of the vehicle at time t , respectively. $w(x(t), t)$, which is the vertical displacement of the bridge at the position x and the time t , can be calculated as follows:

$$w(x(t), t) = \mathbf{H}(x(t), t)\mathbf{y}_{br}(t), \quad (5)$$

where, the $\mathbf{H}(x(t), t)$ is established by the Hermite shape function in this study. $r(x)$ is the road profile displacement at position x . In this study, it is expressed as follows based on the inverse fast Fourier transformation [33]:

$$r(x) = \sum_{i=1}^N \sqrt{4S(f_i)\Delta f} \cos(2\pi f_i x + \theta_i), \quad (6)$$

where, N is the number of spatial frequency sampling points, f_i is the spatial frequency, Δf is the spatial frequency sampling interval and θ_i is a phase angle which distributed from 0 to 2π randomly. $S(f_k)$ is expressed in a general form as follows:

$$S(f_i) = S(f_0) \left(\frac{f_i}{f_0}\right)^{-2} (f_{vl} \leq f_i \leq f_{vu}), \quad (7)$$

where, $f_i = 0.1$ cycles/m is the reference spatial frequency. f_{vl} and f_{vu} denote the lower and upper cut-off spatial frequencies related to the

speed and natural frequencies of the vehicle, respectively [36]. $S(f_0)$ can be determined by the level of RSR according to the ISO-8606 specification [37].

Combining Eqs. (1), (3) and (4), the VBCS can be established by [38]:

$$\begin{bmatrix} \mathbf{M}_b & \mathbf{O} & \mathbf{H}_c \mathbf{M}_{v2} \\ \mathbf{O} & \mathbf{M}_{v1} & \mathbf{O} \\ \mathbf{O} & \mathbf{O} & \mathbf{M}_{v2} \end{bmatrix} \begin{bmatrix} \ddot{\mathbf{y}}_{br} \\ \mathbf{Y} \end{bmatrix} + \begin{bmatrix} \mathbf{C}_b & \mathbf{H}_c \mathbf{C}_{v21} & \mathbf{H}_c \mathbf{C}_{v22} \\ \mathbf{O} & \mathbf{C}_{v11} & \mathbf{C}_{v12} \\ -\mathbf{C}_t \mathbf{H}_c^T & \mathbf{C}_{v21} & \mathbf{C}_{v22n} \end{bmatrix} \begin{bmatrix} \dot{\mathbf{y}}_{br} \\ \mathbf{Y} \end{bmatrix} = \begin{bmatrix} \mathbf{H}_c \mathbf{M}_s \\ \mathbf{O} \\ \mathbf{P}_r \end{bmatrix}, \quad (8)$$

where, $\mathbf{K}_t = \begin{bmatrix} K_{t1} & 0 \\ 0 & K_{t2} \end{bmatrix}$, $\mathbf{C}_t = \begin{bmatrix} C_{t1} & 0 \\ 0 & C_{t2} \end{bmatrix}$, $\mathbf{K}_{v22n} = \begin{bmatrix} K_{v11} + K_{t1} & 0 \\ 0 & K_{v21} + K_{t2} \end{bmatrix}$, $\mathbf{C}_{v22n} = \begin{bmatrix} C_{v11} + C_{t1} & 0 \\ 0 & C_{v21} + C_{t2} \end{bmatrix}$, \mathbf{P}_r is related to the road roughness:

$$\mathbf{P}_r = \mathbf{K}_t \begin{bmatrix} r(x_1(t)) \\ r(x_2(t)) \end{bmatrix}. \quad (9)$$

In this study, Eq. (8) will be solved by the generalized single-step time integration method [39]. Then the interaction force \mathbf{P} can be obtained by Eq. (8) with the updated responses of each nodal at the same time instant. It should be noted that the responses obtained before and the vehicle parameters are only used for the calculation of the interaction force \mathbf{P} , i.e., the moving vehicle load (MVL).

Time domain method (TDM), whose process of generating the system matrix is both clear and succinct, has higher precision compared to the other methods [40,41]. The main theory of TDM is based on the assumption that the moving force maintains a constant speed within each interval. According to the TDM, the relationships between the interaction forces and two different measurements are formed simply as follows:

$$\begin{bmatrix} \mathbf{r}_b \\ \mathbf{y}_a \end{bmatrix} = \begin{bmatrix} \mathbf{A}_b \\ \mathbf{A}_a \end{bmatrix} \mathbf{P}, \quad (10)$$

where, $\mathbf{r}_b \in \mathbb{R}^{ns}$ represents a bending moment vector at a point of interest, with each element corresponding to the bending moment at a discrete time step. Similarly, $\mathbf{y}_a \in \mathbb{R}^{ns}$ represents an acceleration vector at a point of interest, with each element corresponding to the acceleration at a discrete time step. $\mathbf{A}_b \in \mathbb{R}^{ns \times m}$ and $\mathbf{A}_a \in \mathbb{R}^{ns \times m}$ denote the system matrices between the bending moment and interaction force vectors and ones between the acceleration and interaction force vectors, respectively. More details can be found in Ref [7].

Due to the substantial difference in magnitudes between bending moment and acceleration, they should be normalized to achieve dimensionless units prior to their utilization:

$$\begin{bmatrix} \mathbf{r}_b / \|\mathbf{r}_b\| \\ \mathbf{y}_a / \|\mathbf{y}_a\| \end{bmatrix} = \begin{bmatrix} \mathbf{A}_b / \|\mathbf{r}_b\| \\ \mathbf{A}_a / \|\mathbf{y}_a\| \end{bmatrix} \mathbf{P}, \quad (11)$$

where, $\|\cdot\|$ is the Euclidean norm of a vector.

For brevity, Eq. (11) can be rewritten as:

$$\mathbf{y} = \mathbf{AP}, \quad (12)$$

where, $\mathbf{y} \in \mathbb{R}^{2ns}$ and $\mathbf{A} \in \mathbb{R}^{2ns \times m}$ denote the structural responses and the system matrix between structural responses and interaction force $\mathbf{P} \in \mathbb{R}^m$. The dimension of these variables can be changed according to the boundary condition of the bridge, the type of structural response, and the number of responses. However, it has no impact on the following derivations so that $\mathbf{y} \in \mathbb{R}^{2ns}$, $\mathbf{A} \in \mathbb{R}^{2ns \times m}$ and $\mathbf{P} \in \mathbb{R}^m$ are adopted.

2.2. A novel PCA-based dictionary reconstructed for moving vehicle load identification

To tackle the ill-posedness of the solution to Eq. (12), the dictionary theory has also been used in this study. Based on this theory, the vehicle load \mathbf{P} can be expressed in another domain:

$$\mathbf{P} = \mathbf{D}\boldsymbol{\alpha}, \quad (13)$$

where, $\mathbf{D} \in \mathbb{R}^{m \times n}$ and $\boldsymbol{\alpha} \in \mathbb{R}^n$ are the dictionary and atom coefficients related to \mathbf{D} , respectively. If there are n_f interaction forces, Eq. (13) can be re-formed as:

$$\begin{bmatrix} \mathbf{P}_1 \\ \mathbf{P}_2 \\ \vdots \\ \mathbf{P}_{n_f} \end{bmatrix} = \begin{bmatrix} \mathbf{D}_1 & & & \\ & \mathbf{D}_2 & & \\ & & \ddots & \\ & & & \mathbf{D}_{n_f} \end{bmatrix} \begin{bmatrix} \boldsymbol{\alpha}_1 \\ \boldsymbol{\alpha}_2 \\ \vdots \\ \boldsymbol{\alpha}_{n_f} \end{bmatrix}, \quad (14)$$

where, \mathbf{D}_i and $\boldsymbol{\alpha}_i$ are the dictionary and atom coefficient for the i th interaction force, respectively. It should be noted that the domains expressed for different vehicle loads should be distinct. If the matrix \mathbf{D} is not block diagonal, the basis function in each sub-matrix \mathbf{D}_i will influence each other, significantly affecting the atom coefficients $\boldsymbol{\alpha}$. Therefore, when the matrix \mathbf{D} is block diagonal, the basis functions corresponding to other vehicle loads will be vectors consisting of zeros, which do not have any effect.

The selection of the atom in dictionary \mathbf{D} plays an important role in the expression of solution [25]. The dictionaries constructed by sine and cosine functions are the most used in load identification due to its uniform expression [17,23,28,42]. It has also been introduced in MFI which is combined with the rectangular functions, and has great expression in the simulated forces which is composed of sine functions and exponential functions [17]. However, it still exists a distance between this simulation and the real engineering. The information of the vehicle load should be extracted to design the dictionary.

Principal component analysis (PCA) is a method employed to decrease the dimensionality of datasets [43]. Through a set of principal components derived from the training data in each class, the main characteristics of each class can be obtained. In this study, the PCA is used to extract the prior information of the interaction force \mathbf{P} which is obtained in the Section 2.1. In general, the PCA method transforms the data of interest, i.e., the interaction force \mathbf{P} in this study, from a m -dimensional space into a novel d -dimensional space which consists of the PCs [44]:

$$\mathbf{P}_i = \mathbf{B}\boldsymbol{\alpha}_i, \quad (15)$$

where, \mathbf{P}_i and $\boldsymbol{\alpha}_i$ represent the i th interaction force and i th atom coefficient, respectively. \mathbf{B} , which consists of the principal components (PC), are the eigenvectors corresponding to the d largest eigenvalues of the

matrix, thereby constituting the PCA-based dictionary. It is a diagonal matrix on the covariance matrix of the data $\Lambda = E[\mathbf{P}_i\mathbf{P}_i^T]$ [45]:

$$\hat{\Lambda} = \mathbf{B}\mathbf{S}\mathbf{B}^T, \quad (16)$$

where, \mathbf{S} is a diagonal matrix with the sorted eigenvalues $\lambda_1 \geq \lambda_2 \geq \dots \geq \lambda_d$. It can be found that each PC is orthogonal to the others, which rigorously meets the basis function criteria within the dictionary. It should be noted that the first PC in \mathbf{B} , which is always the mean of the dataset, is replaced with a normalized unit vector \mathbf{I}_{norm} . In this study, the training data of the interaction forces is generated according to five levels of road roughness as shown in Fig. 2, which are 'A', 'B', 'C', 'D' and 'E', corresponding to 'very good', 'good', 'average', 'poor' and 'very poor', respectively [34]. In each level of road roughness, 100 training data, whose related road roughness are totally different from the others but in the same level, are generated. Therefore, there are 500 training data generated for one PCA-based dictionary. More details will be discussed in the numerical simulations.

For the number of PCs, only the basis associated with eigenvalues $\lambda > 10^{-6}$ are chosen. This is because the ones associated with eigenvalues $\lambda < 10^{-6}$ can be ignored due to their small contribution to the $\sum_{i=1}^d \lambda_i$ [46]. By this measure, the dimension m of the original space will be reduced into d , rendering the solutions less susceptible to noise interference and leading to more accurate results. Therefore, the truncated PCA-based dictionary \mathbf{B} represents the dictionary \mathbf{D} in Eq. (13). In the following study, the cumulative contribution of PCs in different groups is more concerned. A cumulative ratio (CR) of the PCs can be defined [47]:

$$CR = \frac{\sum_{j \in g_i} \lambda_j}{\sum_{k=1}^d \lambda_k}, \quad (17)$$

where, g_i is the index set related to the i th group.

In total, combining Eqs. (12) and (13) yields:

$$\mathbf{y} = \mathbf{AD}\boldsymbol{\alpha} = \mathbf{W}\boldsymbol{\alpha}. \quad (18)$$

2.3. Newly grouping and weighting strategy for group sparse optimization

For the regularization technology, a penalty term is added to the least-squares method to address the ill-posedness of the inverse problem. This penalty term must be carefully selected based on the form of the solution. Typically, the l_2 -norm penalty is more suitable for dense solutions, while the l_1 -norm penalty is better suited for sparse solutions [48]. For the PCA theory defined in Section 2.2, the atom coefficients as expressed in Eq. (18) cannot be definitively classified in the form of either sparse or dense form. Even though the eigenvalue of each PC has been known based on the PCA technology, the form of solution will differ from the training data due to variations in road surface roughness

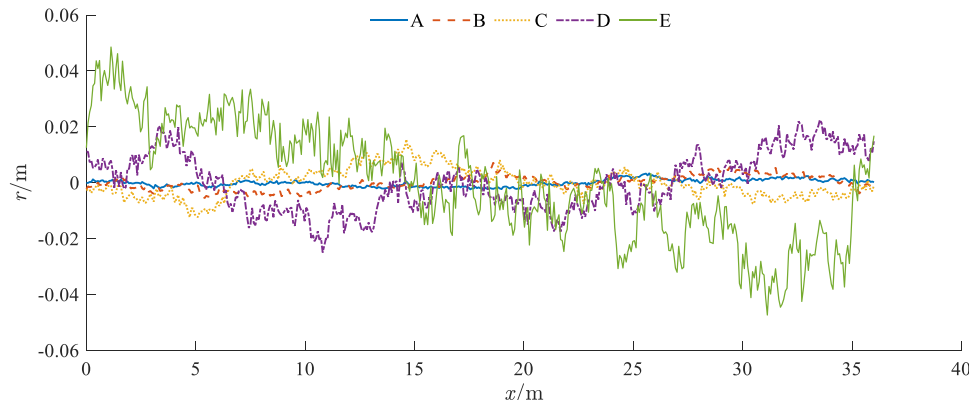


Fig. 2. Five levels of road roughness.

and vehicle type, which are not present in the training data, as well as the noise. Therefore, a group sparse optimization with mixed l_{2-1} regularization based on a newly grouping and weighting strategy is proposed to solve Eq. (18). At first, it is assumed that α is an unknown sparse group of solutions. If α is separated into s groups, it can be reorganized as follows:

$$\alpha = [\alpha_{g_1} \quad \alpha_{g_2} \quad \cdots \quad \alpha_{g_s}]^T, \quad (19)$$

where, α_{g_i} is the sub-vector of α indexed by g_i .

Then Eq. (18) can be solved by the following model with the weighted l_{2-1} norm [49]:

$$\min_{\alpha} \|\alpha\|_{w,2,1} \text{ s.t. } \mathbf{W}\alpha = \mathbf{y}, \quad (20)$$

where, $\|\alpha\|_{w,2,1} = \sum_{i=1}^s w_i \|\alpha_{g_i}\|_2$ and $w_i \geq 0$ is the weight of i th group.

Eq. (20) can be transformed into the following equivalent form by introducing another variable \mathbf{z} :

$$\min_{\alpha, \mathbf{z}} \|\mathbf{z}\|_{w,2,1} = \sum_{i=1}^s w_i \|\mathbf{z}_{g_i}\|_2 \text{ s.t. } \mathbf{z} = \alpha. \quad (21)$$

It should be noted that the objective function in Eq. (21) is separable into the form of $f(\alpha) + g(\mathbf{z})$ due to its exclusive dependence on the variable \mathbf{z} . Then Eq. (21) can be further transformed into an augmented Lagrangian problem:

$$\min_{\alpha, \mathbf{z}} \|\mathbf{z}\|_{w,2,1} + \frac{\gamma_1}{2} \|\mathbf{z} - \alpha\|_2^2 + \frac{\gamma_2}{2} \|\mathbf{W}\alpha - \mathbf{y}\|_2^2 - \lambda_1^T (\mathbf{z} - \alpha) - \lambda_2^T (\mathbf{W}\alpha - \mathbf{y}), \quad (22)$$

where, γ_1 and γ_2 are penalty term. $\lambda_1 \in \mathbb{R}^n$ and $\lambda_2 \in \mathbb{R}^n$ are multipliers.

Eq. (22) can be solved by the alternating direction method (ADM) [50]. The main theory is to minimize Eq. (22) alternately with respect to α and \mathbf{z} . To be detailed, if Eq. (22) is minimized with respect to α , the terms exclusively involving \mathbf{z} can be treated as a constant term. Then for the α -subproblem, Eq. (22) can be re-formed as:

$$\min_{\alpha} \frac{1}{2} \alpha^T (\gamma_1 \mathbf{I} + \gamma_2 \mathbf{W}^T \mathbf{W}) \alpha - (\gamma_1 \mathbf{z} - \lambda_1 + \gamma_2 \mathbf{W}^T \mathbf{y} + \mathbf{W}^T \lambda_2)^T \alpha, \quad (23)$$

where, \mathbf{I} is an identify matrix. And it can be solved by:

$$\alpha = (\gamma_1 \mathbf{I} + \gamma_2 \mathbf{W}^T \mathbf{W})^{-1} (\gamma_1 \mathbf{z} - \lambda_1 + \gamma_2 \mathbf{W}^T \mathbf{y} + \mathbf{W}^T \lambda_2). \quad (24)$$

The same way can be done for the \mathbf{z} -subproblem, and the following minimization problem can be obtained finally:

$$\min_{\mathbf{z}} \sum_{i=1}^s \left[w_i \|\mathbf{z}_{g_i}\|_2 + \frac{\gamma_1}{2} \left\| \mathbf{z}_{g_i} - \alpha_{g_i} - \frac{1}{\beta_1} (\lambda_1)_{g_i} \right\|_2^2 \right]. \quad (25)$$

Eq. (25) can be solved by the soft thresholding method for each group [51]:

$$\mathbf{z}_{g_i} = \max \left\{ \|\mathbf{r}_i\|_2 - \frac{w_i}{\beta_1}, 0 \right\} \frac{\mathbf{r}_i}{\|\mathbf{r}_i\|_2}, \quad (26)$$

where,

$$\mathbf{r}_i = \alpha_{g_i} + \frac{1}{\gamma_1} (\lambda_1)_{g_i}. \quad (27)$$

Finally, the multipliers λ_1 and λ_2 can be updated:

$$\lambda_1 = \lambda_1 - \eta_1 \gamma_1 (\mathbf{z} - \alpha), \quad \lambda_2 = \lambda_2 - \eta_2 \gamma_2 (\mathbf{W}\alpha - \mathbf{y}), \quad (28)$$

where, η_1 and η_2 are step lengths, respectively.

Due to a fact that the response \mathbf{y} in Eq. (20) always incorporates noise, a termination iteration criterion is defined as follows:

$$\frac{\|\alpha^{(k+1)} - \alpha^{(k)}\|}{\|\alpha^{(k)}\|} < \varepsilon, \quad (29)$$

where, ε is a tolerance related to the noise level.

According to the solution to the α -subproblem and \mathbf{z} -subproblem, it can be found that the choices of the index set g_i for each group play an important role in the accuracy and efficiency. Due to a fact that the first few PCs often capture a significant proportion, it is advisable to select the index set for each group. In this study, it is set as 2^i , which means that the α in Eq. (19) is separated into the following form:

$$\alpha = \begin{bmatrix} \underbrace{\alpha_{1,1}}_{\alpha_{g_1}} \underbrace{\alpha_{2,1}}_{\alpha_{g_2}} \underbrace{\alpha_{2,2}}_{\alpha_{g_2}} \cdots \underbrace{\alpha_{i,1}}_{\alpha_{g_i}} \underbrace{\alpha_{i,2}}_{\alpha_{g_i}} \cdots \underbrace{\alpha_{i,2^i}}_{\alpha_{g_i}} \cdots \underbrace{\alpha_{s,1}}_{\alpha_{g_s}} \cdots \underbrace{\alpha_{s,2^s}}_{\alpha_{g_s}} \end{bmatrix}^T, \quad (30)$$

where, α_{ij} is the j th atom in the i th group and $\alpha_{g_i} = 2^i$. Furthermore, if the number of elements in s th group is smaller than 2^s , then all of them are added into the $(s-1)$ th group. The proposed grouping strategy offers three advantages. Firstly, it can be found that the groups whose CR are relatively large can be distinguished clearly from Eq. (30). The number of PCs, whose CR constitutes a relatively small proportion, has a limited impact on the results. Consequently, the primary features in the data will be utilized to a greater extent by this measure. Secondly, the first atom, which represents the static component of the moving vehicle load, can be distinguished from the others. And there is only one element in this group for each axle weight. Thirdly, it is challenging to separate the noise in the measurements, and it significantly affects the identification of atoms, especially in the last group whose CR is smallest.

The weight w_i in Eq. (21), which can be considered as the regularization parameter, is also a difficult problem [52–54]. If the weight w_i is relatively small, its related α_{g_i} will be large. If the weight w_i is relatively large, its related α_{g_i} will be small. In this study, the weight w_i is obtained combining with the eigenvalues of the corresponding PCs in each group:

$$w_i = \left(\frac{\text{num}(g_i) \sum_{j \in g_i} \lambda_j}{\sum_{j \in g_i} \lambda_j} \right)^{1/2}, \quad (31)$$

where, $\text{num}(\cdot)$ is the number of elements, $\sum_{j \in g_i} \lambda_j$ is the last group with the smallest CR . The weights calculated by Eq. (31) are correlated with the cardinality of each group. Due to these measures, the differences in weights among groups will be amplified, especially for the first and last groups. The static weight is the major component of the vehicle load, and the proposed weighting strategy can leverage this prior knowledge.

The above methodology is developed for one interaction force. For two or more interaction forces in this study, the index set g_i of each group should be chosen concurrently from the PCs established independently for each of forces.

Finally, the flowchart of the proposed MLI framework combining the novel PCA-based dictionary with newly grouping and weighting strategy is shown as in Fig. 3.

3. Numerical simulation analysis

To evaluate the feasibility of the proposed approach for MLI, a series of numerical simulations are performed using a VBCS model depicted in Fig. 1. The parameters of the beam-like bridge are as follows: $EI = 2.3 \times 10^{10}$ N·m², $L = 36$ m, $\rho = 5 \times 10^3$ kg/m [36]. The first five natural frequencies of the bridge, such as 2.59 Hz, 10.40 Hz, 23.39 Hz, 41.59 Hz and 64.98 Hz, respectively, are used in this study, and their corresponding damping ratios are all set to be 0.02.

Three half vehicle models in Refs [36,55] and [56] are used to validate the proposed method, with their corresponding vehicle parameters listed in Table 1. And the half vehicle model in Ref [36] is used to construct the PCA-based dictionary. The vehicle's velocity is set to 15 m/s, resulting in a total time of 2.4 s.

The first five PCs and typical eigenvalues of the diagonal matrix \mathbf{S} in Eq. (16) are shown in Fig. 4. Fig. 4(a)–(e) illustrate the shape of the first five PCs within the time domain. The eigenvalues of the first 30 PCs are

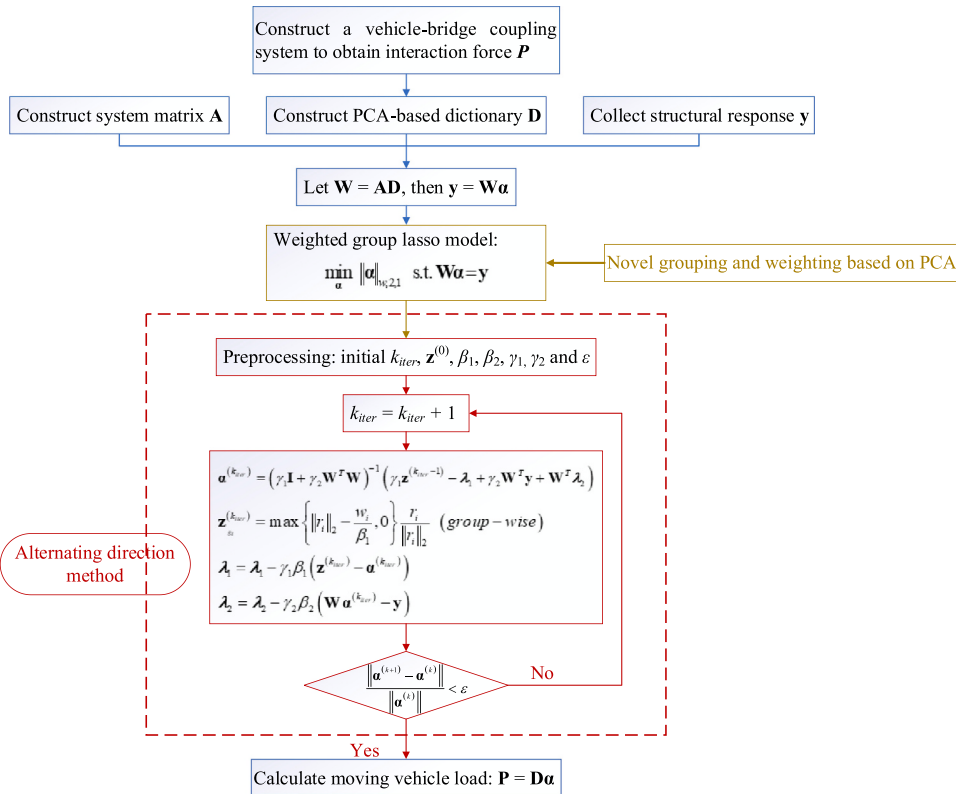


Fig. 3. Flowchart of proposed MLI framework using novel PCA-based dictionary and newly grouping and weighting strategy.

Table 1

Parameters of bridge-vehicle models in traditional references.

Refs	$I_v/\text{kg}\cdot\text{m}^2$	m_v/kg	S/m	a_1	a_2	m_1/kg	$K_{s1}/\text{N/m}$	$C_{s1}/\text{N/m/s}$	$K_{r1}/\text{N/m}$	$C_{r1}/\text{N/m/s}$	m_2/kg	$K_{s2}/\text{N/m}$	$C_{s2}/\text{N/m/s}$	$K_{r2}/\text{N/m}$	$C_{r2}/\text{N/m/s}$
[36]	9.5×10^5	16200	4.27	0.567	0.433	700	4×10^5	1×10^4	1.75×10^6	3.9×10^3	1.1×10^6	1×10^6	2×10^4	3.5×10^6	4.3×10^3
[55]	1.3×10^4	1×10^4	5	0.4	0.6	600	1.16×10^5	2.5×10^4	7.85×10^5	0.1×10^3	1000	3.73×10^5	3.5×10^4	1.57×10^6	0.2×10^3
[56]	2896	2000	2.6	0.461	0.539	45	1.7×10^4	3000	2.5×10^5	0	25	1.5×10^5	3000	2.5×10^5	0

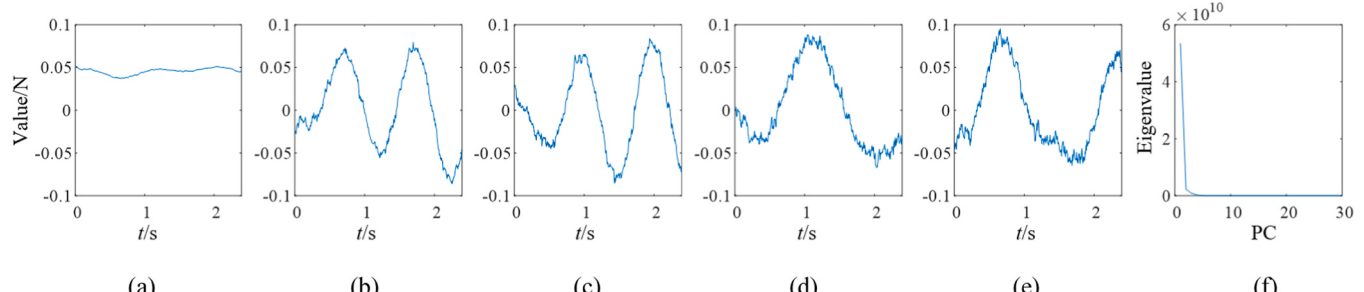


Fig. 4. The PCA of the model in Ref [36]: (a)-(e) the first five PCs, and (f) typical eigenvalues.

shown in sub-figure Fig. 4(f). It can be found that the contribution of the first PCs far exceeds that of the remaining basis. Furthermore, the first PC as showed in sub-figure (a), is comparatively close to a constant vector compared with other basis functions. It is typical for the first PC to exhibit a shift in its values, as the vehicle is modeled as a system with both elastic and damping properties. Additionally, the road surface roughness is considered in this study, further influencing this shift. This is why the first PC is replaced with a normalized unit vector in this

article. The other PCs denote the dynamic component of the interaction force. Compared with the atoms of trigonometric functions in Ref [17], they are more related to the vehicle model and road roughness. After ignoring the PCs with eigenvalues $\lambda < 10^{-6}$, the PCA-based dictionaries for the front and rear axles consist of only 471 and 478 PCs, respectively. Based on the grouping and weighting strategy proposed in Section 2.3, the group number is eight, and their corresponding CRs are as follows: 4.20×10^{11} , 1.55×10^{10} , 2.03×10^9 , 2.41×10^8 , 1.74×10^8 ,

8.52×10^7 , 1.94×10^7 and 1.31×10^6 . It can be found that the CR of the first group is larger than the others groups, particularly in comparison to the last one. According to Eq. (31), the corresponding weight of each group can be calculated as follows: 0.0025, 0.0184, 0.0720, 0.2953, 0.4920, 0.9937, 2.9480 and 26.3629. It can be found that the weight of the last group is larger than the first one significantly. Therefore, the most significant information of the vehicle can be extracted, while the atoms in the groups with small CRs, which are more sensitive to noise, are penalized.

To emulate the effects of measurement noise contaminated in practice, white noise is incorporated into each noiseless response \mathbf{y}_i to emulate the noisy response \mathbf{y}_i^n [24]:

$$\mathbf{y}_i^n = \mathbf{y}_i + \mathbf{N}_{\text{noise}} \times \frac{1}{ns} \sum_{i=1}^{ns} |\mathbf{y}_i| \times \text{rand}, \quad (32)$$

where, $\mathbf{N}_{\text{noise}}$ and rand are the noise level and a standard normal distribution vector, respectively.

To evaluate the precision of the proposed method, a relative percentage error (*RPE*) is calculated between the identified force \mathbf{P}_{iden} and true one \mathbf{P}_{true} as follows:

$$RPE = \frac{\|\mathbf{P}_{\text{iden}} - \mathbf{P}_{\text{true}}\|}{\|\mathbf{P}_{\text{true}}\|} \times 100\%. \quad (33)$$

The proposed method is based on structural responses caused by moving vehicle loads. Therefore, when discussing the identified results, it is essential to specify which measured responses were used to obtain these results. In this study, the employed responses are either bending moments or accelerations or their combinations, and are represented by the response locations and types. For instance, the notation ‘3/4 m&5/8a’ indicates that the response combinations from both the bending moment at the 3/4 span of the bridge and acceleration at 5/8 span are employed for MLI, here symbols m and a indicate bending moment and acceleration responses respectively. Moreover, similar representations are used in the other cases.

3.1. Comparative studies on three methods

The half vehicle model in Ref [36] is utilized to assess the effectiveness of the proposed method at first. In order to distinguish it from the original training data in PCA, the interaction force \mathbf{P} is obtained under another reconstructed road surface roughness with the class of ‘C’ (RSR ‘C’) which is totally different from the training data. Furthermore, the weight of vehicle body m_v is changed to 24300 kg to simulate the gross vehicle weight.

The MFI methods from Refs [24] and [28], namely the NRAMP and ASS-BOMP methods, are used to compare with the proposed method in this study. For the NRAMP method, two adjustable parameters are settled as $\varepsilon_2 = 1 \times 10^{-4}$ and $\varepsilon_3 = 0.8$ here. Furthermore, the dictionary in this method, which is composed of trigonometric functions and rectangular functions, is denoted as TR dictionary in the following for simplicity. To make the comparison fairly, the numbers of atoms in the TR and the PCA-based dictionary should be similar in a reasonable way. Therefore, the highest frequency of interest for moving loads is settled as 40 Hz so that there are 1160 atoms in this dictionary, which has been a redundant dictionary for SRP. For the ASS-BOMP method, the PCA-based dictionary is used as the same as the proposed method. Due to a fact that there are no rules of weights and grouping settled in this method, the group number is settled as 80 and the related block length is 12. It should be noted that the number of PCs constructed by the model in Ref [36] is 949 for two interaction forces. The surplus atoms are represented by the zero vector for the ASS-BOMP method.

For the proposed method, the parameters for ADM are settled as follows: $\gamma_1 = \gamma_2 = 1.618$, $\beta_1 = 0.3/\text{mean}(|\mathbf{y}|)$ and $\beta_2 = 3/\text{mean}(|\mathbf{y}|)$ [50]. Where, $\text{mean}(\cdot)$ denotes the mean value of vector. The tolerance ε in Eq. (29) is settled as 1×10^{-6} at first. The *RPE* values generated by three

methods are compared in Table 2 across different response combinations and noise levels. The comparison on the true vehicle loads and ones identified by the Proposed, ASS-BOMP and NRAMP methods are also shown in Fig. 5 under RSR ‘C’, ‘1/2 m&3/4 m&3/8a’ and 1 % noise level.

From Table 2, it can be found that the ASS-BOMP method fails to accurately identify the true axle loads in the response combination of ‘1/2 m&5/8a’ and ‘1/2 m&3/4 m&3/8a’. Especially in the response combination of ‘1/2 m&5/8a’, only the *RPE* value of the identified rear axle load is not greater than 100 % but it still remains considerably high at 92.91 % under 1 % noise level. From Fig. 5, it can be found that the fluctuation of the ASS-BOMP method is relatively serious in the whole domain comparing with the other methods for both vehicle axle loads. This is because the ASS-BOMP method is specifically designed to solve the block sparse problem. But the atom coefficients of the PCA-based dictionary do not exhibit sparsity in the same manner.

For the NRAMP method, the *RPE* values under ‘1/2 m&5/8a’ are smaller compared to those of the ASS-BOMP method. Nevertheless, they all surpass 11.7 %, contrasting with the proposed method where the highest *RPE* is only 6.03 %. From Fig. 5, even though the fluctuation of the identified results by the NRAMP method is relatively stable comparing with the ASS-BOMP method, it is totally not coincided with the true axle load. This discrepancy arises from the difficulty of the TR dictionary in expressing interaction forces, which are fundamentally different from the simulated forces comprised solely of trigonometric functions in this study.

For the proposed method, the *RPE* values under all response combinations are lower than the other two methods. The highest *RPE* value is merely 6.03 % under ‘1/2 m&5/8a’ and 5 % noise level. As shown in Fig. 5, comparing with the ASS-BOMP and NRAMP methods, the identified results by the proposed method exhibit greater conciseness with the true axle load for both axles.

From Table 2, it can also be found that as the number of acceleration increases, the accuracy of all methods is improved compared to the case with only one acceleration. This phenomenon can be attributed to the dominance of acceleration in the high-frequency domain, enabling them to better capture dynamic components. For the case that the number used for MLI is limited to two, equivalent to the number of axles, the *RPE* values for all methods increase. For example, under a noise level of 1 %, the most accurate *RPE* value for the rear axle load \mathbf{P}_2 under ‘1/2 m&5/8a’ is 4.34 % using the proposed method. However, this accuracy is improved to 1.67 % for the same axle load and noise level when three measurements are utilized for MLI. Therefore, employing a greater number of accelerometers and responses exceeding the number of vehicle axles can effectively enhance identification accuracy.

Table 2
RPE values by three methods under different cases (RSR ‘C’).

Response combination	Noise level	Proposed method		ASS-BOMP		NRAMP	
		$\mathbf{P}_1/\%$	$\mathbf{P}_2/\%$	$\mathbf{P}_1/\%$	$\mathbf{P}_2/\%$	$\mathbf{P}_1/\%$	$\mathbf{P}_2/\%$
1/2 m&5/8a	1 %	5.63	4.34	*	92.91	16.28	11.95
	2 %	5.58	4.42	*	*	17.06	12.42
	5 %	6.03	4.91	*	*	14.69	11.78
1/2 m&3/8a&5/8a	1 %	1.89	1.67	5.79	5.26	7.86	5.73
	2 %	2.29	1.82	5.27	6.39	8.29	5.98
	5 %	3.89	2.97	11.27	7.65	7.94	6.44
1/2 m&3/4 m&3/8a	1 %	3.79	3.22	38.84	33.29	11.93	9.00
	2 %	3.91	3.26	*	74.77	10.62	10.41
	5 %	5.56	4.04	*	*	13.48	9.91

* indicates *RPE* value exceeds 100 %.

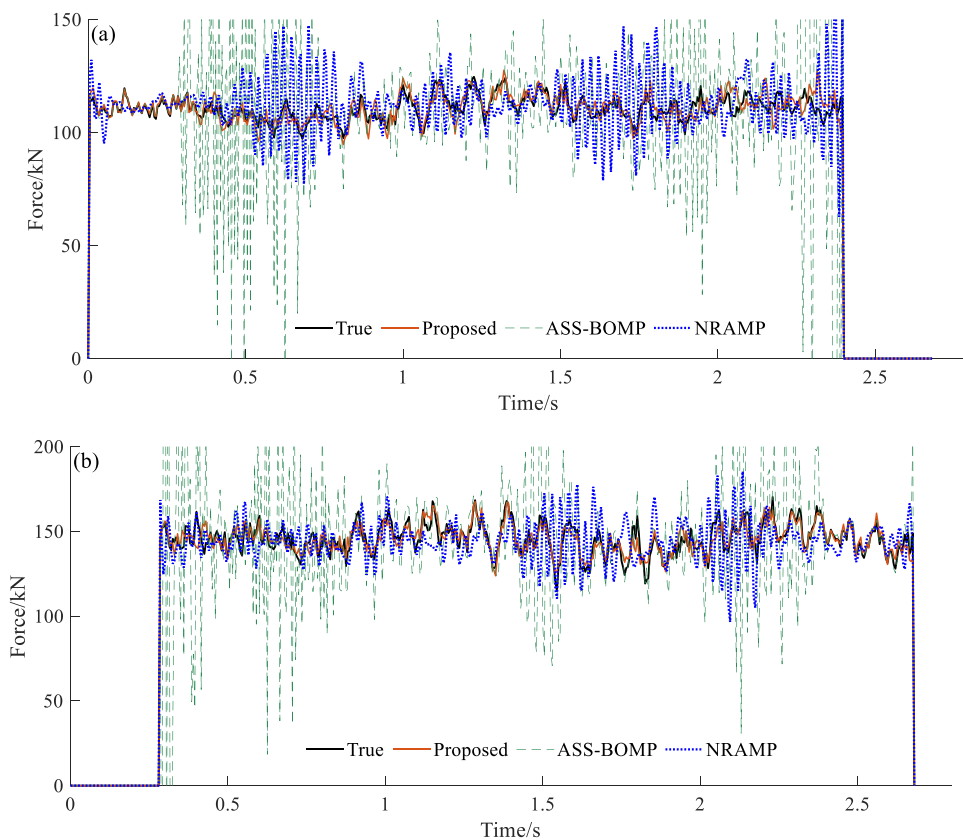


Fig. 5. Comparison on true vehicle loads and ones identified by Proposed, ASS-BOMP and NRAMP methods ('1/2 m&3/4 m&3/8a', 1 % noise level, 'C' RSR). (a) Front axle load P_1 . (b) Rear axle load P_2 .

3.2. Effects of road surface roughness (RSR)

To further investigate the accuracy of the proposed method, the interaction forces under the RSRs of classes 'B' and 'D' are used in this part. Comparison on *RPE* values by three methods under the '1/2 m&3/4 m&3/8a' and RSR 'D' are listed in Table 3 firstly. In a high noise level of 5 %, the *RPE* values of the ASS-BOMP method exceed 100 %, indicating failure. This outcome is similar to what was observed in the case of RSR 'C'. In contrast, the *RPE* values of the NRAMP method are kept within 12.4 %, outperforming the ASS-BOMP method. However, the proposed method achieves the highest accuracy across all noise levels, maintaining a *RPE* value of just 9.02 % even under a high noise level of 5 %.

The MLI results by the NRAMP, ASS-BOMP and proposed methods are illustrated in Fig. 6 under the '1/2 m&3/4 m&3/8a', 1 % noise level and RSR 'D'. The same conclusion can be drawn as in the RSR 'C' in Fig. 5, indicating that the proposed method exhibits superior capability in identifying the true axle load compared to the other two methods. For the ASS-BOMP method, the fluctuation of identified forces under RSR 'D' is still serious and exhibits similarity with the identified results under RSR 'C'. For the NRAMP method, the fluctuation of identified results is stable but smaller than the true axle load for the heavier rear axle load

P_2 . This is because the NRAMP method exhibits a strong robustness to noise so that the parts of the dynamic component of interaction force are denoted as noise to be reduced.

Comparative study of the proposed method under the RSR of classes 'B', 'C' and 'D' are listed in Table 4. From Table 4, it can be found that all the *RPE* values under different noise levels and response combinations increase as the severity of road conditions increases. For example, under '1/2 m&5/8a' and 1 % noise level, the *RPE* values of P_1 and P_2 are merely 2.83 % and 2.61 %. However, when considering the same situation with RSR 'D', these values increase to 8.66 % and 7.78 %, respectively. This is because the fluctuation of the interaction forces under RSR 'D' in Fig. 6 is larger than that under RSR 'C' in Fig. 5.

Furthermore, it can be found that the impact of RSRs on accuracy is more severe compared to the influence of noise levels in some cases. For example, under '1/2 m&5/8a' and 1 % noise level, the *RPE* value of P_1 is 5.63 % for RSR 'C'. With the RSR increases, the *RPE* value increases to 8.66 %, surpassing the impact caused by the elevated noise level in the same response combination, which leads to a 6.03 % increase. This situation is observed across all cases under '1/2 m&5/8a' and '1/2 m&3/8a&5/8a', yet remains absent in the case of '1/2 m&3/8a&5/8a'. It means that the RSR is also a factor that cannot be ignored, especially when the number of measurements used for MLI, particularly the number of acceleration, is relatively small.

In total, the proposed method demonstrates high accuracy across different RSRs. In addition to noise levels and the number of sensors used for MLI, RSR is also a key factor that needs to be carefully considered in influencing accuracy.

3.3. Effects of number of training data

In the above sections, the number of training data used for constructing the PCA-based dictionary was 500, including 100 training data

Table 3

Comparison on *RPE* values by three methods ('1/2 m&3/4 m&3/8a', RSR'D).

Noise level	Proposed method		ASS-BOMP		NRAMP	
	$P_1/\%$	$P_2/\%$	$P_1/\%$	$P_2/\%$	$P_1/\%$	$P_2/\%$
1 %	6.97	6.01	31.50	33.60	11.61	12.19
2 %	7.37	6.32	74.93	76.24	11.89	12.28
5 %	9.02	7.36	*	*	12.10	12.34

* indicates *RPE* value exceeds 100 %.

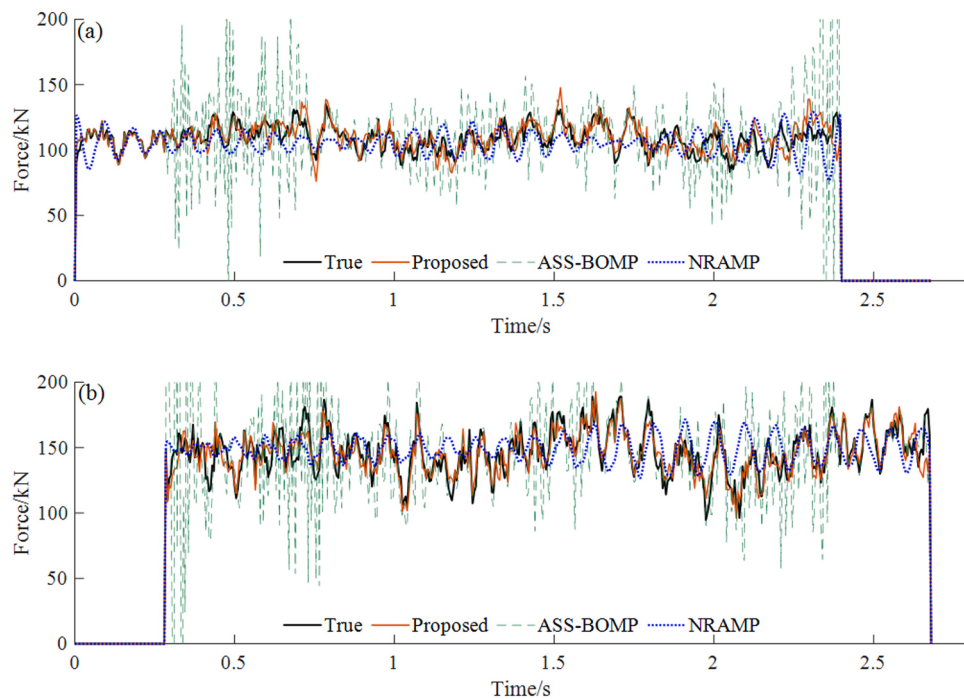


Fig. 6. Comparative MLI results by three methods ('1/2 m&3/4 m&3/8a', 1 % noise level, RSR 'D'). (a) Front axle load P_1 . (b) Rear axle load P_2 .

Table 4
Comparison on RPE values by the proposed methods under different cases.

Response combination	Noise level	$P_1/\%$			$P_2/\%$		
		'B'	'C'	'D'	'B'	'C'	'D'
1/2 m&5/8a	1 %	2.83	5.63	8.66	2.61	4.34	7.78
	5 %	3.52	6.03	9.59	2.74	4.91	8.40
1/2 m&3/8a&5/8a	1 %	0.93	1.89	3.83	0.88	1.67	3.55
	5 %	2.60	3.89	7.10	2.08	2.97	5.33
1/2 m&3/4 m&3/8a	1 %	1.93	3.79	6.97	1.72	3.22	6.01
	5 %	3.26	5.56	9.02	2.95	4.04	7.36

generated for each one of five RSR levels labeled by 'A', 'B', 'C', 'D' and 'E', respectively. To explore the effects of number of training data, four different numbers of training data are taken into consideration in this section. Except of the 100 training data, the additional 50, 75 and 200 training data are also generated for each level of RSR. Therefore, there are four cases with 250, 375, 500 and 1000 training data in total for determining an appropriate number of training data to construct the corresponding PCA-based dictionaries. To distinguish each generated one for four cases, which are denoted as 'PCs I', 'PCs II', 'PCs III' and 'PCs IV' cases respectively, they are ordered from fewer to more numbers of training data. **Table 5** lists the RPE values corresponding to different numbers of training data under 'RSR' C and 5 % noise level.

From **Table 5**, it can be found that even with the smallest dataset (Case of PCs I, with 250 training data), the highest RPE value is only 10.36 % under the '1/2 m&5/8a'. This indicates that the proposed

method still holds an advantage compared to the ASS-BOMP and NRAMP methods. Additionally, it is evident that the response combination still has an impact on the results. The identified results for the '1/2 m&5/8a', which only uses two responses, are the least accurate across all cases. In contrast, the results for the '1/2 m&3/8a&5/8a' are the best.

In addition, one can find that the RPE values will be decreased with the increase of training data. For example, under the case of '1/2 m&3/8a&5/8a', the RPE values for the case of PCs II (375) are 4.63 % and 4.78 % respectively for the first and second axles, which are smaller than 6.60 % and 6.04 % for PCs I (250). Moreover, when the number of training data increases to PCs IV (1000), the RPE values for two axles are only 3.36 % and 2.38 %. Comparing with the RPE values of 3.89 % and 2.97 % for PCs III (500), the improvement in accuracy is not so significant although the RPE values decrease with the increase in the number of training data as well. Under this condition, it is unnecessary to further increase the training data. Although the PCs IV (1000) can provide higher accuracy, it demands a large amount of data. Taking the above into consideration, it is more appropriate to select the 500 training data. Therefore, the following analysis is based on the PCA-based dictionary constructed using 500 training data without loss of generality.

3.4. Effects of grouping and weighting

In [Section 3.1](#), we have found that the proposed method exhibits higher accuracy compared with the ASS-BOMP method using mean grouping. In this section, the impact of grouping and weighting on the proposed method is further explored specifically under different RSRs and noise levels. The comparative method is employed with mean

Table 5
RPE values under four cases (RSR 'C', 5 % Noise).

Response combination	PCs I (250)		PCs II (375)		PCs III (500)		PCs IV (1000)	
	$P_1/\%$	$P_2/\%$	$P_1/\%$	$P_2/\%$	$P_1/\%$	$P_2/\%$	$P_1/\%$	$P_2/\%$
1/2 m&5/8a	10.36	8.26	6.00	5.03	6.03	4.91	6.30	4.65
1/2 m&3/8a&5/8a	6.60	6.04	4.63	4.78	3.89	2.97	3.36	2.38
1/2 m&3/4 m&3/8a	9.60	8.08	5.76	4.45	5.56	4.04	5.00	3.78

grouping and identical weights for each group, but the calculation algorithm is ADM which is the same as the proposed method. It means that the α_{g_i} in Eq. (30) and the w_i in Eq. (31) in each group are equal, respectively.

According to Eq. (30), the proposed method under PCA-based dictionary is divided into 8 groups. To ensure a fair comparison, the block length (bl) under mean grouping for the comparative method is set as 120, 80 and 60, respectively, corresponding to group numbers of 8, 12, and 16, which are called as 'ADM I', 'ADM II', and 'ADM III' methods in the following comparison to distinguish them from the proposed method. The identified results by these methods under the '1/2 m&3/4 m&3/8a' are listed in Table 6.

From Table 6, it can be found that when the noise level is low, the grouping and weights strategy employed in the proposed method show no significant improvement compared to the other methods. For example, under RSR 'D' and 1 % noise level, the RPE values obtained from the proposed method for each axle load, 6.97 % and 6.01 % respectively, are comparable to those of the ADM III method, which are 4.75 % and 5.71 %. However, its group number is 16, which is significantly larger than the 8 groups utilized in the proposed method, allowing for a more detailed representation of atoms within each group.

With the increase of noise level, the RPE values of the proposed method are significantly smaller compared to those of the other methods. For example, under 5 % noise level and RSR 'B', the RPE values of the proposed method are 3.26 % and 2.95 % for each axle, respectively. But the RPE values for the ADM I method, which has the same group number as the proposed method, are 17.05 % and 28.98 %, respectively. These differences are substantial when compared to the values obtained by the proposed method. The ADM III method, exhibits RPE values more than two times higher than those obtained by the proposed method in a high noise level of 5 %. From Fig. 7, it can be found that all comparative methods exhibit noticeable deviations from the truth in their identification results in the whole-time domain especially for the lighter front axle P_1 . It means that the proposed novel grouping and weighting strategy can enhance stability and robustness to noise. As a result, the proposed method can provide more accurate identification even under high-noise levels.

3.5. Effects of different vehicle models and tolerances

As discussed above, the simulated vehicle model is related to the training data of PCA-based dictionary. Even though another RSR model and weight of vehicle mass are conducted to simulate the real vehicle model, they still exhibit a similar fluctuation. In this part, another two vehicle models as listed in Table 1 are used to validate the proposed method. The RPE values of the proposed method under the response combination of '1/2 m&3/4 m&3/8a' for different vehicle models are listed in Table 7.

From Table 7, it can be found that even though the PCA-based dictionaries reconstructed by the vehicle model in Ref [36] can still explain

the other vehicle loads reasonably, particularly when the noise level is below 5 %. This is because the reconstructed PCA-based dictionary is complete and capable of representing any clean signal along the same dimension. Even though with the increase of RSR, the proposed method can still identify the vehicle load reasonably when it is under 1 % and 2 % noise levels respectively. For example, under 1 % and 2 % noise levels, the RPE values of the vehicle model in Ref [56] are controlled in 6.30 %. However, when the noise level escalates to 5 %, the RPE values increase significantly, particularly under RSR 'B', with RPE values of 31.95 % and 34.70 % for each axle of the vehicle model in Ref [56], respectively. The same conclusion cannot be drawn in the Ref [55], but the RPE value has increased to 9.34 % and 12.54 % for each axle under RSR 'D' and 5 % noise level.

Actually, this situation can be handled by the tolerance ε in Eq. (29) due to a fact that they are set to mitigate the impact of noise. In the former study, it is settled as $\varepsilon = 1 \times 10^{-6}$ for all cases. For subsequent investigations, it has been adjusted to 1×10^{-5} and 5×10^{-4} . Table 8 lists the RPE values under different tolerances ε in the case of '1/2 m&3/4 m&3/8a' and RSR 'C'.

From Table 8, it can be found that when the tolerance decreases to 5×10^{-4} , the RPE values of each axle under 5 % noise level significantly decrease to 14.57 % and 14.13 % for the vehicle model in Ref [56]. However, for the vehicle models in Refs [36] and [55], the RPE values both exceed 43 %, with the RPE value of rear axle P_2 are higher than 77 % for the vehicle model in Ref [55]. When ε is settled as 1×10^{-5} , the identified results of the vehicle model in Ref [56] can be improved greatly. Under the 5 % noise level, the RPE values of each axle decrease to only 3.96 % and 4.89 %, respectively. For the other two vehicle models, the results under $\varepsilon = 1 \times 10^{-5}$ are slightly worse compared to those under $\varepsilon = 1 \times 10^{-6}$ at a noise level of 1 %. But under the 5 % noise level, the results are comparable. For example, the RPE value of the front axle P_1 is 5.56 % under $\varepsilon = 1 \times 10^{-6}$ which is larger than 5.01 % under $\varepsilon = 1 \times 10^{-5}$. Conversely, the RPE value of the rear axle P_2 is 4.04 % under $\varepsilon = 1 \times 10^{-6}$ which is slightly smaller than 4.72 % under $\varepsilon = 1 \times 10^{-5}$. The identified forces under different tolerances ε for the vehicle model in Ref [36] under '1/2 m&3/4 m&3/8a', 1 % noise level and RSR 'C' are also shown in Fig. 8. It can be found that when ε is set as 5×10^{-4} , the identified results have deviated significantly from the true load. And it does not align with the priori information that the load is fluctuates around the true static weight [57]. The results under $\varepsilon = 1 \times 10^{-6}$ and $\varepsilon = 1 \times 10^{-5}$ are closer to the true axle load.

In Table 9, the calculation costs under different tolerances are further investigated. It can be found that with the increase of noise level, the calculation cost increase in all cases. For example, under $\varepsilon = 1 \times 10^{-6}$ and 1 % noise level, the calculation cost is 9.651 s for the vehicle model in Ref [36]. Under the same conditions but with 5 % noise level, the calculation cost increases to 10.078 s. Furthermore, the calculation cost decreases as ε increases across all vehicle models. When the tolerance is set as $\varepsilon = 1 \times 10^{-5}$, the calculation costs under all cases have been obviously improved compared to those under $\varepsilon = 1 \times 10^{-6}$. Even

Table 6
Comparison of RPE values by different grouping and weighting.

RSR	Noise level	Proposed method		ADM I		ADM II		ADM III	
		P_1	P_2	P_1	P_2	P_1	P_2	P_1	P_2
'B'	1 %	1.93	1.72	1.95	3.05	1.59	2.38	1.49	2.06
	2 %	2.19	1.82	2.82	4.80	2.48	3.74	2.27	3.17
	5 %	3.26	2.95	17.05	28.98	15.87	24.87	13.82	20.62
'C'	1 %	3.79	3.22	2.98	4.31	2.71	3.89	2.60	3.53
	2 %	3.91	3.26	4.59	7.51	3.90	5.86	3.49	4.95
	5 %	5.56	4.04	17.84	28.41	15.75	24.21	13.2	19.98
'D'	1 %	6.97	6.01	4.57	5.93	4.85	5.84	4.75	5.71
	2 %	7.37	6.32	6.24	9.03	6.00	7.73	5.77	7.29
	5 %	9.02	7.36	19.46	33.49	17.85	29.91	16.16	26.54

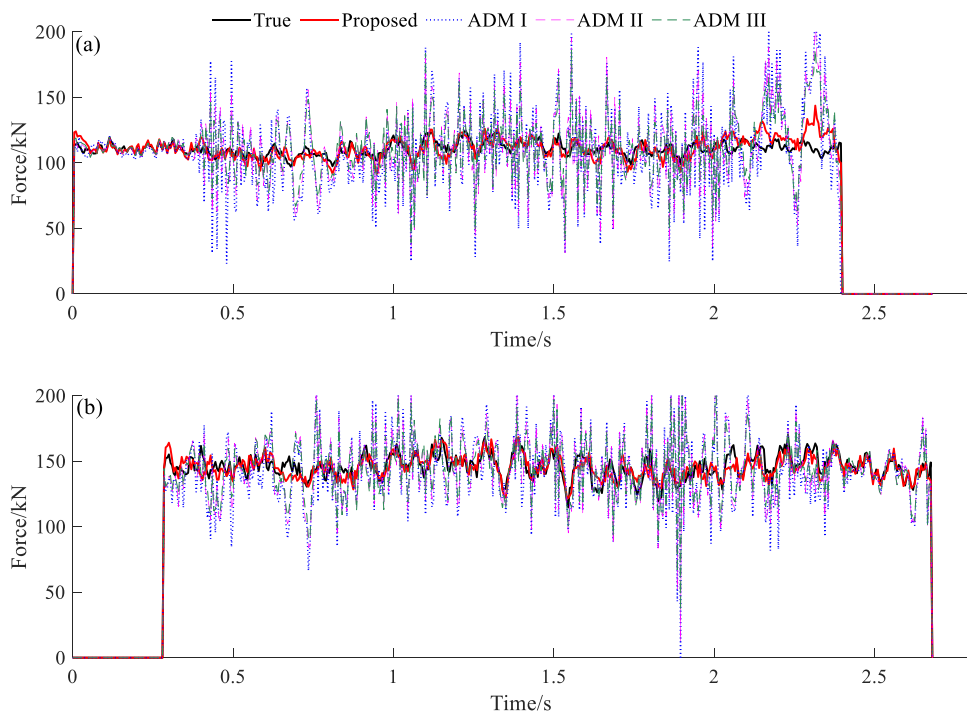


Fig. 7. Comparative MLI results on grouping and weighting ('1/2 m&3/4 m&3/8a', 5 % noise level, RSR 'C'). (a) Front axle load P_1 . (b) Rear axle load P_2 .

Table 7

Comparison of RPE values for different vehicle models under '1/2 m&3/4 m&3/8a'.

RSR	Noise level	Ref[36]		Ref[55]		Ref[56]	
		P_1	P_2	P_1	P_2	P_1	P_2
'B'	1 %	1.93	1.72	1.70	3.05	1.63	1.87
	2 %	2.19	1.82	1.82	3.19	1.83	2.19
	5 %	3.26	2.95	3.64	4.86	31.95	34.70
'C'	1 %	3.79	3.22	3.00	4.84	3.22	3.53
	2 %	3.91	3.26	3.41	5.04	3.15	3.78
	5 %	5.56	4.04	4.78	6.30	28.06	34.09
'D'	1 %	6.97	6.01	5.64	8.74	6.01	6.18
	2 %	7.37	6.32	5.94	9.05	6.18	6.30
	5 %	9.02	7.36	9.34	12.54	27.60	29.19

Table 8

Comparison of RPE values under different tolerances for different vehicle models ('1/2 m&3/4 m&3/8a', RSR 'C').

Noise level	ϵ	Ref[36]		Ref[55]		Ref[56]	
		P_1	P_2	P_1	P_2	P_1	P_2
1 %	1×10^{-6}	3.79	3.22	3.00	4.84	3.22	3.53
	1×10^{-5}	4.68	4.09	3.82	5.41	3.33	3.72
	5×10^{-4}	43.73	46.84	55.70	77.61	16.09	13.65
5 %	1×10^{-6}	5.56	4.04	4.78	6.30	28.06	34.09
	1×10^{-5}	5.01	4.72	5.29	5.96	3.96	4.89
	5×10^{-4}	43.88	47.06	55.60	77.54	14.57	14.13

though the calculation costs under $\epsilon = 5 \times 10^{-4}$ are smaller than in other cases, the identified results corresponding to them are worst in most cases as observed previously.

Therefore, if the type of vehicle model can be determined for constructing the PCA-based dictionary, $\epsilon = 1 \times 10^{-6}$ is the best choice for accuracy, albeit with increased calculation costs, especially in the low noise levels of 1 %. $\epsilon = 1 \times 10^{-5}$ is more suitable in different vehicle models, as it significantly reduces calculation costs compared to

$\epsilon = 1 \times 10^{-6}$ while still maintaining reasonable accuracy.

4. Experimental validations

4.1. Experimental setup

To validate the feasibility of the proposed method, a simulation of a model vehicle moving on a hollow beam bridge is carried out. As shown in Fig. 9(a), the whole bridge includes three parts, such as leading beam, main beam and trailing beam, respectively. The model vehicle, as in Fig. 9(b), is connected to a motor through a traction rope. Its wheelbase is 0.33 m. The measurement area is located on the main beam with a span of 3 m. Its cross section, as shown in Fig. 9(c), is a hollow rectangle whose width and height are 0.15 m and 0.05 m, respectively, with a wall thickness of only 0.002 m. The density of unit length and flexural stiffness are $\rho = 7.62 \text{ kg}\cdot\text{m}$ and $EI = 7.94 \times 10^4 \text{ N}\cdot\text{m}^2$, respectively.

A finite element model (FEM) with elastic supporting in Ref [24] is established for updating the raw FEM. Then the first three frequencies are updated as 19.56 Hz, 73.09 Hz and 162.30 Hz, respectively. Three strain gauges are installed at the 1/4, 1/2 and 3/4 spans of the bridge. The relationship between measurement strains and bending moments are established based on the updated FEM model. They exhibit a linear relationship between bending moments and strains at 1/4, 1/2 and 3/4 spans with linear coefficients as $2.849 \text{ N}\cdot\text{m}\cdot\mu\epsilon^{-1}$, $2.813 \text{ N}\cdot\text{m}\cdot\mu\epsilon^{-1}$ and $3.065 \text{ N}\cdot\text{m}\cdot\mu\epsilon^{-1}$, respectively [58].

Seven accelerometers are installed in the 1/8, 1/4, 3/8, 1/2, 5/8, 3/4 and 7/8 spans of the bridge. After all the strain and acceleration are acquired at a sampling rate of 2048 Hz, a low-pass Butterworth filter is applied to filter all the responses, and the collected data are also resampled as 512 Hz for convenient storage and subsequent MFI computation.

To detect the velocity of the model vehicle in each part, seven photoelectric sensors are installed, and the distance between each photoelectric sensor is 0.5 m. As shown in Fig. 9(b), it can be found that two iron wires are positioned above the two axles of the model vehicle. They can obscure the light transmitted by the photoelectric sensors so that the moment when each axle moves across different photoelectric sensors

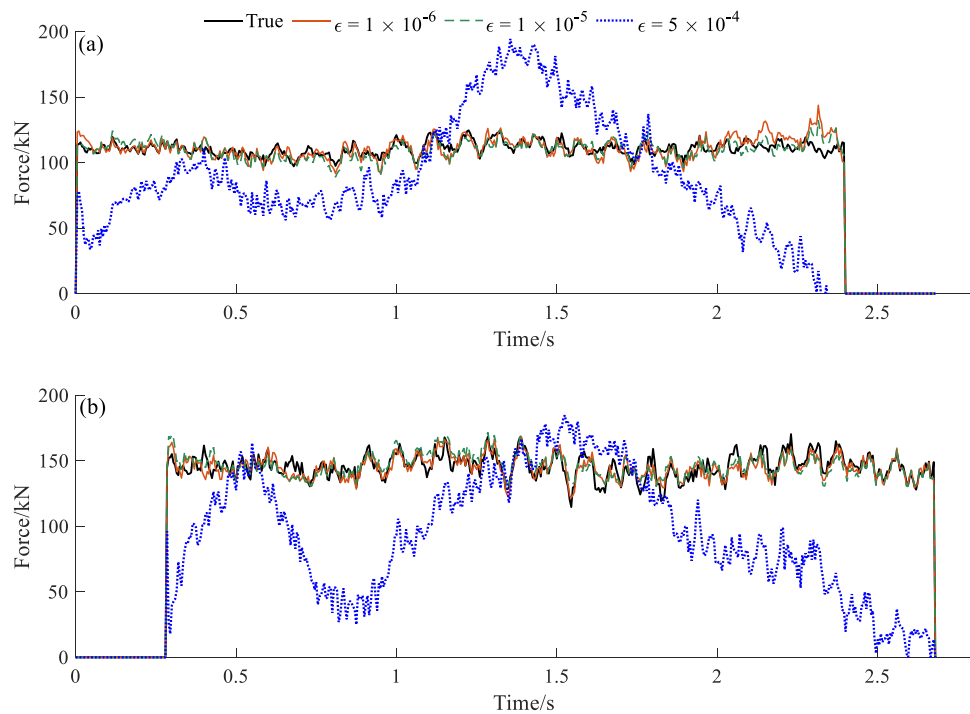


Fig. 8. Comparative MLI results by three tolerances ('1/2 m&3/4 m&3/8a', 1 % noise level, RSR 'C'). (a) Front axle load P_1 . (b) Rear axle load P_2 .

Table 9

Comparison of calculation cost under different tolerances for different vehicle models ('1/2 m&3/4 m&3/8a', RSR 'C', unit: s).

Noise level	ϵ	Ref[36]	Ref[55]	Ref[56]
1 %	1×10^{-6}	9.651	5.353	1.289
	1×10^{-5}	5.611	3.442	0.887
	5×10^{-4}	0.242	0.161	0.329
5 %	1×10^{-6}	10.078	5.423	13.526
	1×10^{-5}	5.858	3.462	0.853
	5×10^{-4}	0.237	0.159	0.301

can be recorded.

A recorded impulsive signal of photoelectric sensors is shown as in Fig. 10(a), which indicates that the vehicle moved across the beam at a mean velocity of 1.38 m/s during the whole-time domain. Furthermore,

the initial and final impulsive signals correspond to moments when the model vehicle arrives at and departs from the main beam, respectively. Therefore, the distance travelled that the model vehicle moves on the bridge is divided into six parts. The system matrix A in Eq. (12) is reconstructed for the following MLI based on the assumption that the velocity of vehicle is unchanged in each part.

The collected strain and acceleration are also shown in Fig. 10 (b) and (c). It can be found that before the vehicle arrives at the bridge, the collected data of accelerometers exhibits obvious changes. This is because the leading beam and the main beam are both installed on the same support and directly connected to each other.

Due to the limitation of experimental instruments, the dynamic load of vehicle is difficult to obtain directly. However, the static weight of each axle can be weighed in advance so that a relatively percentage value of axle weight (*RPEw*) is defined to validate the proposed method

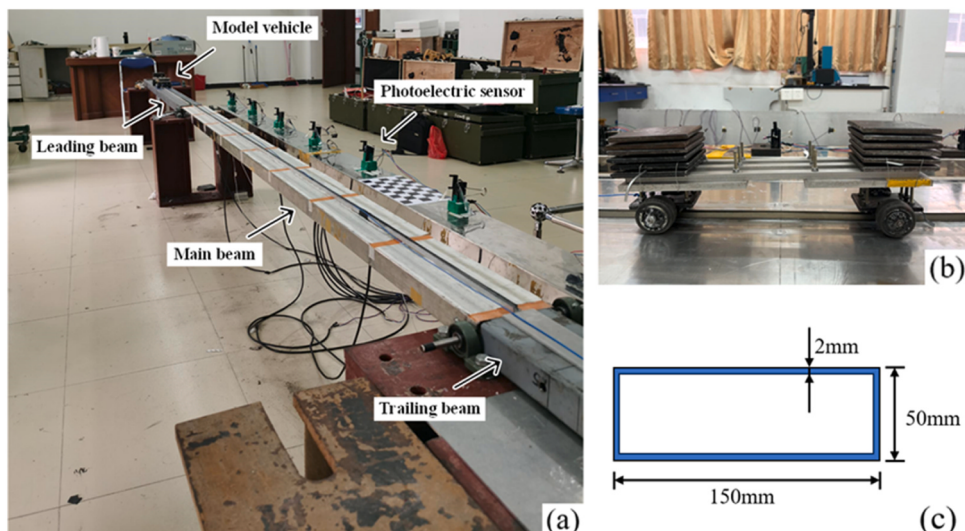


Fig. 9. Experimental setup. (a) Vehicle-bridge model. (b) Model vehicle. (c) Cross section of beam.

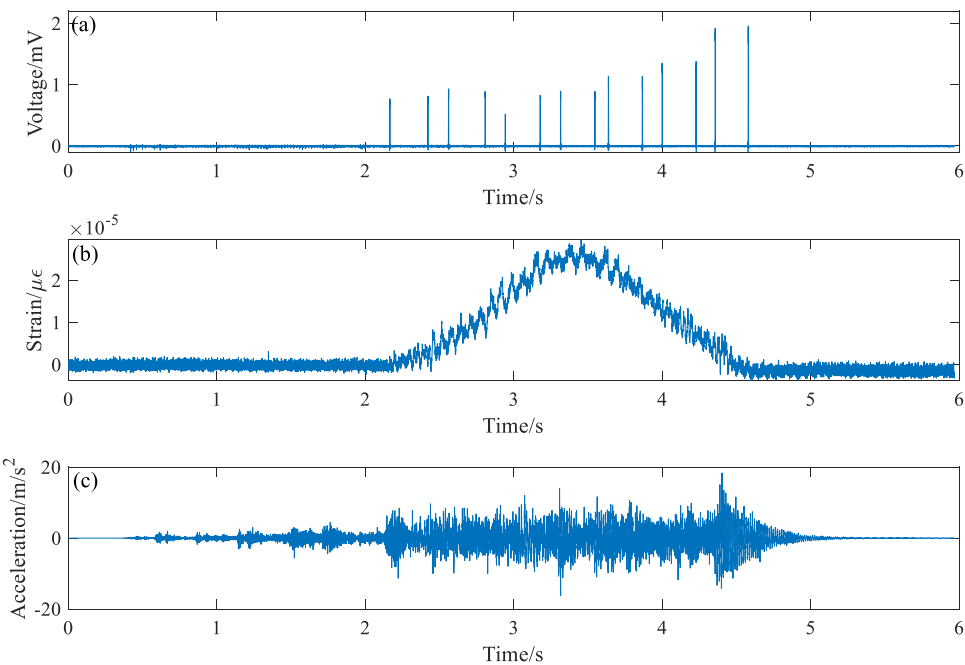


Fig. 10. Typical measured signals as two-axle vehicle crosses main beam. (a) Photoelectric signals. (b) Strain response. (c) Acceleration.

in this part:

$$RPEW = \frac{|fs_{true} - fs_{iden}|}{fs_{true}} \times 100\% \quad (34)$$

where, fs_{true} and fs_{iden} are the true and identified static axle weights, respectively. The fs_{iden} is calculated by:

$$fs_{iden} = I_{norm}\alpha_1, \quad (35)$$

where, I_{norm} is the element in a normalized unit vector \mathbf{I}_{norm} , and α_1 is the first atom coefficient corresponding to the first group, representing the static component of the moving vehicle load. There is only one element in this group for each axle weight.

The accelerometer utilized in the experiment is the PCB-333B30, with a frequency range ranging from 0.5 Hz to 3000 Hz. Consequently, it cannot capture static signals due to its inability to detect the static component. This is because the first principal component in the PCA-based dictionary corresponds to the static component of the vehicle load with a frequency of 0 Hz, and there is no corresponding atom coefficient for the first principal component. Moreover, the proposed weighting strategy assigns a small weight to this component, resulting in a large corresponding coefficient, which can negatively impact the accuracy of the results. Hence, the first PCs in the PCA-based dictionary, which were initially normalized unit vectors, are replaced with zero vectors for acceleration in experiments.

The vehicle parameters of the model vehicle cannot be determined due to the limitation of experiments. Therefore, a dynamic scale-model is used to construct the PCA-based dictionary. The parameters of bridge and vehicle models in numerical simulations are used to be the original real models. According to the similarity law of VBCS in Ref [59,60], the similar scales of vehicle stiffness λ_s and damping λ_d can be obtained as follows:

$$\begin{cases} \lambda_s = \lambda_l \cdot \lambda_E \\ \lambda_d = \lambda_E \cdot \lambda_l^{1/2} \cdot \lambda_u \end{cases}, \quad (36)$$

where, λ_l , λ_E and λ_u are geometric scale, elastic modulus scale and deformation scale, respectively. They are settled as 1/12, 1/50 and 1/12 respectively, based on the ratio of the scale model and the original real model. For example, the span of bridge in the numerical simulations and

the experiment are 36 m and 3 m, respectively, resulting in a geometric scale is $\lambda_l = 1/12$. The deformation scale is set as the same as geometric scale. The settlement of elastic modulus scale is influenced by the bridge materials and natural frequencies. However, the bridge parameters used in the numerical simulation, which are derived from Ref [36], only include information about flexural stiffness. Since the moment of inertia and Young's modulus of the material were not known in detail, the elastic modulus scale is artificially set to 1/50 in this study. For the similar scale of vehicle mass λ_m , it is set as 6.24×10^{-4} due to the total mass of model vehicle is almost 110 N in experiment. According to dimensional analysis, the similar scale of I_v is set as:

$$\lambda_l = \lambda_m \cdot \lambda_{ls}^2, \quad (37)$$

where, λ_{ls} is the wheelbase scale, which is set as 7.73×10^{-2} based on the wheelbase in the numerical simulation and experiment, which are 4.27 m and 0.33 m, respectively.

According to Eqs. (36) and (37), the parameters of vehicle used for constructing PCA-based dictionary are listed in Table 10. The first axle of the model vehicle load under different road roughness conditions is shown in Fig. 11. The figure demonstrates that the fluctuations become more pronounced with increasing road surface roughness. Additionally, it is observed that all training data fluctuates around the static weight, which aligns with the real engineering.

Under the mean velocity of 1.38 m/s used as in Fig. 10, the first five PCs and typical eigenvalues are also shown in Fig. 12. The first PC appears relatively smooth compared to the others, leading to its consideration as the static component of MVL, consistent with the phenomenon observed in the numerical simulation. Furthermore, it can be found that the eigenvalues of first five PCs are significantly larger than the others, indicating that their corresponding PCs represent the main characteristic of the vehicle load. These phenomena indicate that

Table 10
Vehicle parameters used for constructing PCA-based dictionary.

$I_v = 3.5383 \text{ kg}\cdot\text{m}^2$	$m_1 = 0.4365 \text{ kg}$	$m_2 = 0.6859 \text{ kg}$
$m_y = 10.1020 \text{ kg}$	$K_{s1} = 666.67 \text{ N/m}$	$K_{s2} = 1666.67 \text{ N/m}$
$S = 0.33 \text{ m}$	$K_{f1} = 2916.67 \text{ N/m}$	$K_{f2} = 5833.33 \text{ N/m}$
$a_1 = 0.567$	$C_{s1} = 4.8113 \text{ N/m/s}$	$C_{s2} = 9.6225 \text{ N/m/s}$
$a_2 = 0.433$	$C_{f1} = 1.8764 \text{ N/m/s}$	$C_{f2} = 2.0688 \text{ N/m/s}$

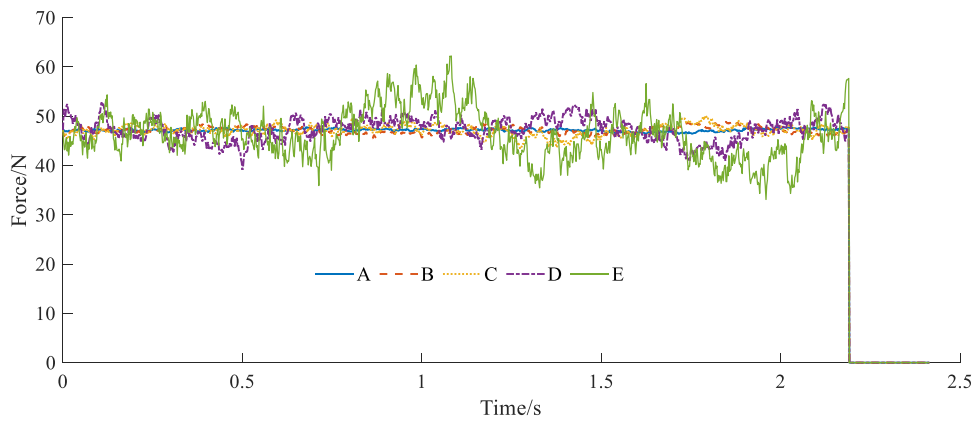


Fig. 11. Training data under different road surface roughness.

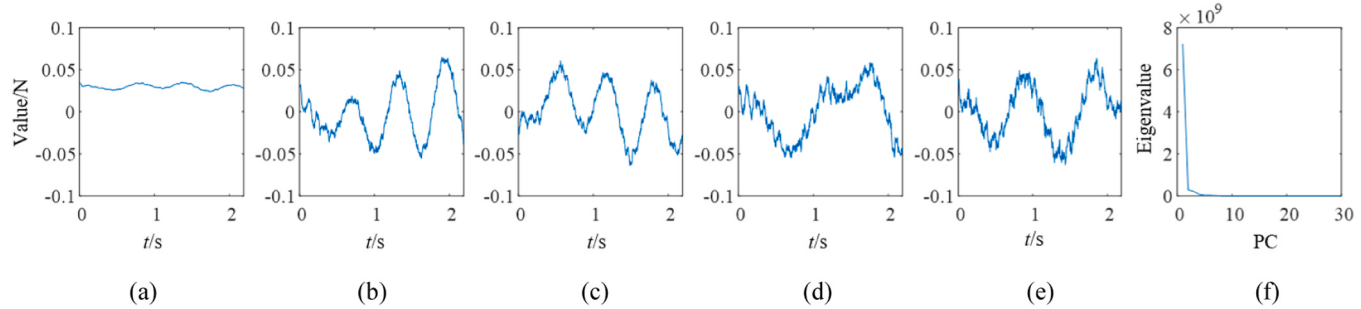


Fig. 12. PCA of model vehicle load based on similarity law of VBCS. (a)-(e) The first five PCs. (f) Typical eigenvalues.

the similarity law used to obtain the training data has been successful so far. After ignoring the PCs with eigenvalues $\lambda < 10^{-6}$, the PCA-based dictionaries for each axle load contain only 500 PCs. According to the newly grouping and weighting strategy proposed in Section 2.3, there are eight groups according to Eq. (30). Their corresponding weights calculated according to Eq. (31) are as follows: 0.0094, 0.0370, 0.1512, 0.3035, 0.5221, 1.2027, 3.3757 and 27.3130, which shows that the last

group is penalized more severely, especially compared to the first group.

4.2. Identified results and discussion

In this part, some experimental scenarios have been devised to assess the feasibility of the proposed method. At first, the mean velocity of model vehicle is set as 1.38 m/s. The static axle weights for the front and

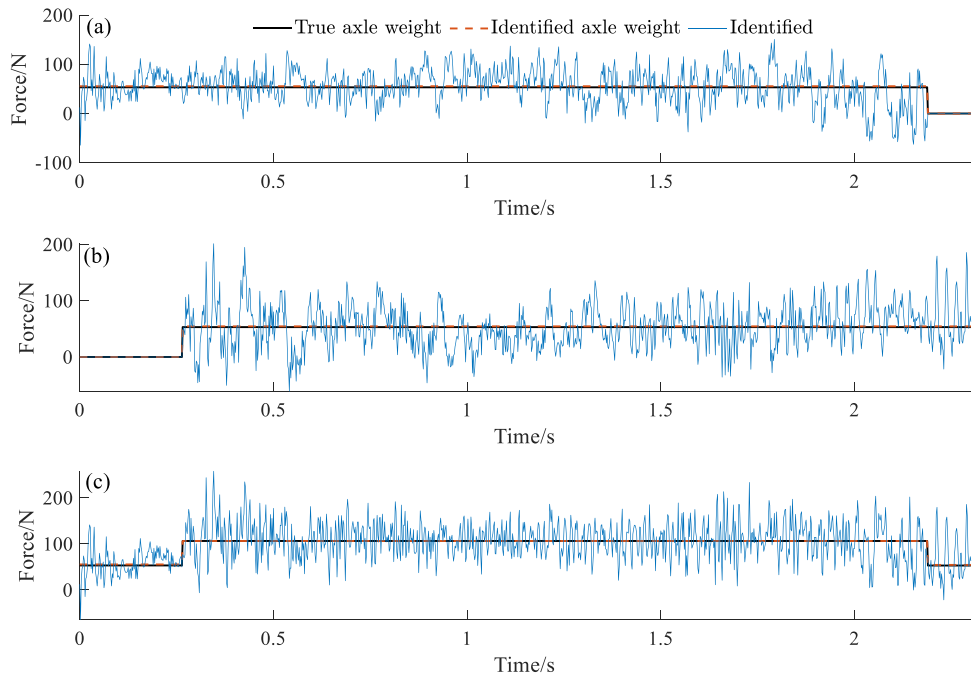


Fig. 13. Identified results under '1/2 m&3/4 m&3/8a' by proposed method. (a) Front axle load P_1 . (b) Rear axle load P_2 . (c) GVW.

rear axles are 53.27 N and 53.08 N, respectively, and the gross vehicle weight (GVW) of the model vehicle is 106.35 N. The tolerance ε of the proposed method is set as 1×10^{-5} and the other parameters are the same as in the numerical simulations. The response combination of '1/2 m&3/4 m&3/8a' is used firstly to validate the propose method. The identified results are 55.44 N and 54.43 N for each axle with the *RPE* value of 4.07 % and 2.53 %. The identified total weight is 109.88 N and the corresponding *RPE* value is only 3.30 %. The identified results are also shown in Fig. 13.

From Fig. 13, one can find that the identified results for both the front and rear axle loads, as well as GVW, fluctuate around their corresponding true axle weight. They are in agreement with the priori information in Ref [57], indicating that the dynamic components of the moving vehicle load fluctuate around the corresponding static weight. However, as shown in Fig. 13, the identified results are less than zero in few time intervals. This is due to the sensitivity of the inverse problem to noise. On one hand, the data collected during the experimental process is inherently affected by noise. On the other hand, even though the updated finite element model of the bridge is used in the experimental validation, the positions of each axle at each time step are another crucial element to construct the system matrix A. They are estimated under the assumption that the vehicle moves at a constant velocity over each part of the bridge. As a result, these positions may deviate significantly from the true ones, especially at a high sampling frequency of 512 Hz.

In addition, the effects of selection of tolerance ε are also considered here. Table 11 lists the identified results and calculation cost for different tolerances under '1/2 m&3/4 m&3/8a' and the mean velocity of 1.38 m/s. In the numerical simulation, the results show that the calculation cost is small but the accuracy is the worst under $\varepsilon = 5 \times 10^{-4}$. From Table 11, the same conclusion can be drawn. For example, the *RPE* value of the identified weight of rear axle is 10.59 % which is the largest among all cases. Additionally, the tolerance $\varepsilon = 1 \times 10^{-5}$ is suggested to be more suitable for various vehicle models due to its comparable accuracy and shorter calculation cost compared to the case of $\varepsilon = 1 \times 10^{-6}$ in the numerical simulation. From Table 12, it can be found that the calculation cost under $\varepsilon = 1 \times 10^{-5}$ can be reduced greatly comparing with $\varepsilon = 1 \times 10^{-6}$. For the identification of static load, even though the *RPE* value of the rear axle is 2.53 % for $\varepsilon = 1 \times 10^{-5}$, it is higher than the 0.53 % for $\varepsilon = 1 \times 10^{-6}$ under the same case, the identified results for the front axle and GVW with $\varepsilon = 1 \times 10^{-5}$ are both more accurate than those of $\varepsilon = 1 \times 10^{-6}$.

The identified results under different tolerances ε are shown in Fig. 14 for further analysis under '1/2 m&3/4 m&3/8a'. From Fig. 14, it is evident that the identified results for $\varepsilon = 1 \times 10^{-6}$ and $\varepsilon = 1 \times 10^{-5}$ exhibit significant overlap for all axles and GVW, while the identified results for $\varepsilon = 5 \times 10^{-4}$ are notably different. For the front axle, it seems that the identified result of $\varepsilon = 5 \times 10^{-4}$ has some low-order harmonic component throughout the entire time domain. A similar observation

Table 11
Comparative studies under different tolerance ε .

Tolerances ε	Front axle P_1 / N		Rear axle P_2 / N		Calculation cost / s
	Identified (True)	Identified RPEw	Identified (True)	Identified RPEw	
1×10^{-6}	57.25 (53.27)	53.37 (53.08)	110.62 (106.35)	53.343	28.615
	7.46%	0.53%	4.00%		
1×10^{-5}	55.44 (53.27)	54.43 (53.08)	109.88 (106.35)	4.07%	0.698
	2.53%	3.30%	2.53%		
5×10^{-4}	57.55 (53.27)	58.71 (53.08)	116.26 (106.35)	8.03%	9.30%
	10.59%	10.59%	9.30%		

Table 12

Comparison on identified results by different methods ('1/2 m&3/4 m&3/8a', mean velocity: 0.80 m/s).

Methods	Front axle P_1 / N		Rear axle P_2 / N		GVW / N	
	Identified (True)		Identified RPEw			
Proposed	50.60 (53.27)	57.75 (53.08)	57.75 (53.08)	57.75 (53.08)	108.35 (106.35)	
ADM I	5.02 % (53.27)	8.80 % (53.08)	8.80 % (53.08)	8.80 % (53.08)	1.87 % (106.35)	
	41.20 (53.27)	68.22 (53.08)	68.22 (53.08)	68.22 (53.08)	108.42 (106.35)	
ADM II	22.66 % (53.27)	28.53 % (53.08)	28.53 % (53.08)	28.53 % (53.08)	2.89 % (106.35)	
	41.21 (53.27)	68.12 (53.08)	68.12 (53.08)	68.12 (53.08)	109.33 (106.35)	
ADM III	22.64 % (53.27)	28.34 % (53.08)	28.34 % (53.08)	28.34 % (53.08)	2.81 % (106.35)	
	41.25 (53.27)	67.91 (53.08)	67.91 (53.08)	67.91 (53.08)	109.16 (106.35)	
	22.57 %	27.93 %	27.93 %	27.93 %	2.64 %	

can be made for the identification of the rear axle under $\varepsilon = 5 \times 10^{-4}$. Furthermore, these harmonic components cannot cancel each other out in the GVW identification. All of the results under $\varepsilon = 5 \times 10^{-4}$ are not in agreement with the prior information mentioned before that the identified results fluctuate around the true axle weight. This corresponds to the findings in the numerical simulation as shown in Fig. 8. Therefore, $\varepsilon = 1 \times 10^{-5}$ emerges as the optimal choice, offering higher accuracy and reduced calculation cost in experiment validations. The same conclusion, supported by numerical simulations, is also evident in the experimental results for the proposed method.

Moreover, the impact of grouping and weighting on the proposed method is also further assessed in the experiment. For the comparative methods, the block length (bl) under meaning grouping is set as 125, 100 and 50, and their corresponding group number are 8, 10 and 20 respectively. These comparative methods are denoted as 'ADM I', 'ADM II' and 'ADM III' methods in the following. The identified results by these methods and the proposed methods are listed in Table 12 under '1/2 m&3/4 m&3/8a', $\varepsilon = 1 \times 10^{-5}$ and mean velocity of 0.80 m/s. It can be found that even though the identified *RPE* values of GVW by the compared methods are all controlled under 2.90 %, all the static load results obtained from the compared methods are around 41 N and 68 N for both the front and rear axles, which are far lower than the true weight of 53.27 N in the front axle and also far higher than the true of 53.08 N in the rear, respectively. The corresponding identified *RPE* values are all higher than 22.5 % in the front axle and higher than 27.9 % in the rear, respectively, which are both unacceptable in practice. Comparing with these methods, the *RPE* values by the proposed method for each axle can be controlled under 8.8 %, which is a better accuracy in engineering applications.

For further analysis of the results, Fig. 15 presents the correlation matrices of the identified front and rear axle loads for all methods individually. It can be found that all the identified results by ADM I, ADM II and ADM III methods can be conducted the same. Moreover, the correlation coefficients between the identified results by the proposed method and those by the compared methods exceed 92 %. Additionally, as the number of groups increases, the identified results by the compared methods become more similar to those by the proposed method. These results indicate that although the identified moving vehicle loads by the compared method exhibits similarity to ones by the proposed method, the proposed novel grouping and weighting strategy can better identify the static component of the moving vehicle loads. Besides, the effects of different response combinations, axle weights and vehicle speeds on the proposed method are also conducted in laboratory, the corresponding identified results are presented in Table 13.

It can be found from Table 13 that when the weights of each axle are not equaled to each other, it has an impact on the *RPE* values of each axle. For instance, with true axle weights of 48.68 N for the front axle

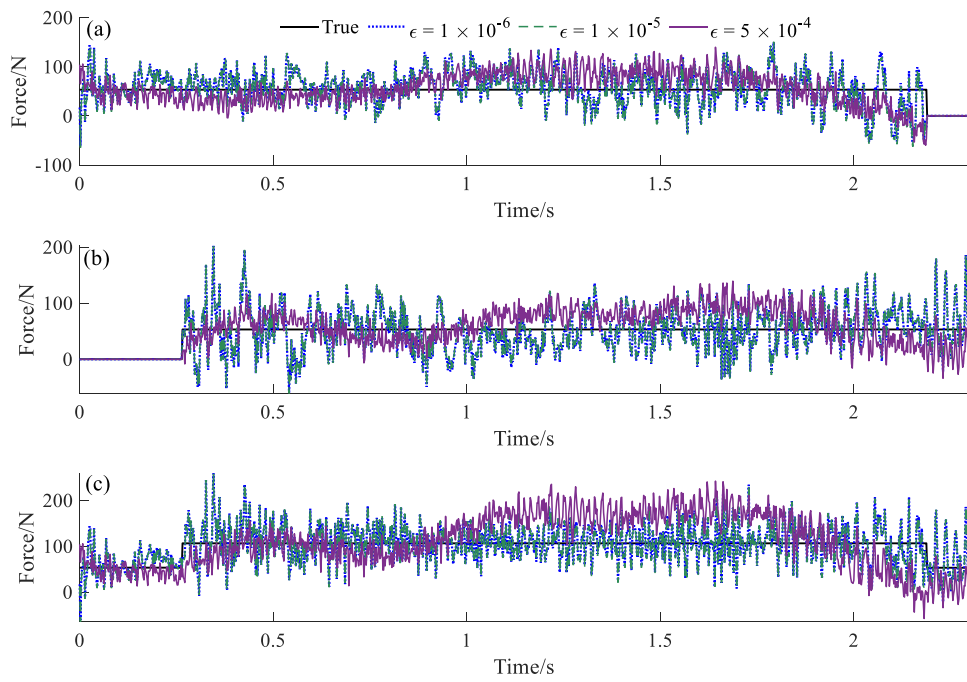


Fig. 14. Identified results by different tolerances. (a) Front axle load P_1 . (b) Rear axle load P_2 . (c) GVW.

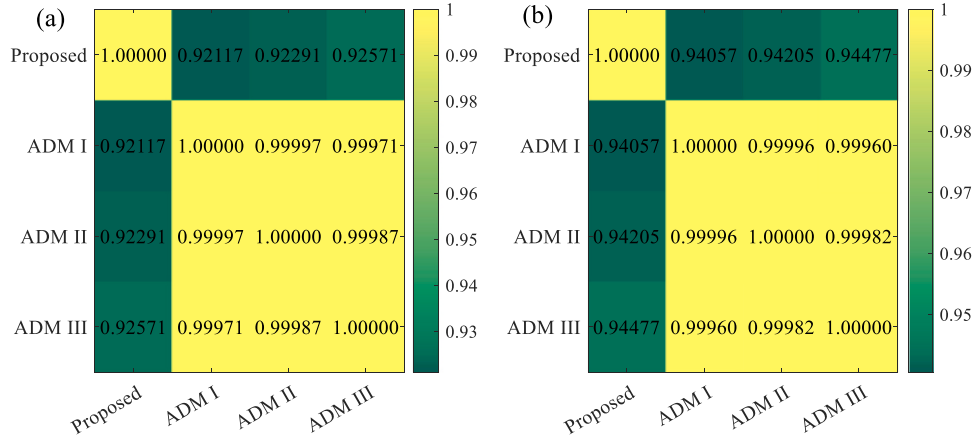


Fig. 15. Correlation matrices from all methods. (a) Front axle load P_1 . (b) Rear axle load P_2 .

and 66.39 N for the rear axle, the corresponding identified results are 52.24 N and 60.27 N, respectively. Similarly, with static axle weights of 65.18 N for the front axle and 50.81 N for the rear axle, the identified results are 57.44 N and 54.05 N, respectively. This is because the PCs for each axle in the same groups are conducted simultaneously during the whole calculation time so that the PCs of each axle cannot be distinctly separated for individual calculations. Additionally, when the mean velocity of the vehicle is lower, the identified GVW tends to be more accurate due to reduced vehicle-bridge interaction effects. However, the RPE values of the identified GVW remain within 7.71 %. It indicates that the similarity law of VBCS used to construct the PCA-based dictionary is reasonable and potential for widespread application in different bridge models.

5. Conclusions

Aiming at the absence of information of moving vehicle loads (MVL) in the dictionary theory and atom characteristics in weighted group sparse model in the existing methods, a novel moving load identification (MLI) framework is proposed for the beam-like bridge structures based

on a novel dictionary derived from the principal component analysis (PCA) and a newly grouping and weighting strategy in this study. The vehicle-bridge coupling system (VBCS) is established at first to obtain interaction forces between the vehicle and bridge. Subsequently, the relationship between these forces and bridge responses is established in time domain. The PCA technique is then employed to construct a novel PCA-based dictionary by extracting the prior information of interaction forces. With the utilization of weighted l_{2-1} norm, the MLI problem is transformed into a weighted group sparse model incorporating newly grouping and weighting. The alternating direction method (ADM) is used to solve this problem based on the newly grouping and weighting strategy. Finally, some numerical simulations and experiments are designed to assess the proposed method. The results demonstrate that:

- 1) Compared with the ASS-BOMP and NRAMP methods, the proposed method exhibits high accuracy. It means that the PCA-based dictionary provides a more effective representation of MVL comparing to the conventional dictionary consisting of trigonometric and rectangular functions. The ADM with newly grouping and weighting

Table 13

Comparative studies on proposed method under different cases.

Response Combination	Mean velocity/ m/s	Front axle P_1 / N		Rear axle P_2 / N		GVW / N
		Identified (True) RPEw	Identified (True) RPEw	Identified (True) RPEw	Identified (True) RPEw	
3/4 m&3/8a&5/ 8a	1.33	52.24	60.27	112.51		
		(48.68) 6.69 %	(66.39) 9.22 %	(115.06) 2.46 %		
3/4 m&3/8a&5/ 8a	1.38	57.44	54.05	111.48		
		(65.18) 11.88 %	(50.81) 6.38 %	(115.99) 3.88 %		
3/4 m&3/8a&1/ 4a	1.38	57.30	57.26	114.56		
		(53.27) 7.56 %	(53.08) 7.87 %	(106.35) 7.71 %		
1/2 m&3/ 4 m&3/8a	1.38	55.44	54.43	109.88		
		(53.27) 4.07 %	(53.08) 2.53 %	(106.35) 3.30 %		
3/4 m&3/8a&5/ 8a	0.80	54.23	54.19	108.42		
		(53.27) 1.78 %	(53.08) 2.08 %	(106.35) 1.93 %		
1/2 m&3/ 4 m&3/8a	0.80	50.60	57.75	108.35		
		(53.27) 5.02 %	(53.08) 8.80 %	(106.35) 1.87 %		

strategy can further enhance identification performance comparing to the existing methods.

- 2) With the increase in noise level and the severity of road surface roughness (RSR), the proposed method can still identify MVL effectively. The newly grouping and weighting strategy proposed in this study enables the proposed method to accurately represent the actual load conditions even in the presence of high levels of noise. Additionally, the proposed strategy enables better identification of the static component in the MVL in the experiment validations. However, the proposed method is still sensitive to the accurate establishment of the system matrix A in Eq. (12), which needs to be addressed in future work.
- 3) Increasing the number of training data improves the accuracy of the identified results. However, the choice of response combination has a

Appendix

$$\begin{aligned}
 \mathbf{M}_{v1} &= \begin{bmatrix} m_v & 0 \\ 0 & I_v \end{bmatrix}; \quad \mathbf{M}_{v2} = \begin{bmatrix} m_1 & 0 \\ 0 & m_2 \end{bmatrix}; \\
 \mathbf{C}_{v11} &= \begin{bmatrix} C_{s1} + C_{s2} & (-C_{s1}a_1 + C_{s2}a_2)S \\ (-C_{s1}a_1 + C_{s2}a_2)S & (C_{s1}a_1^2 + C_{s2}a_2^2)S^2 \end{bmatrix}; \\
 \mathbf{C}_{v12} &= \begin{bmatrix} -C_{s1} & -C_{s2} \\ C_{s1}a_1S & -C_{s2}a_2S \end{bmatrix}; \quad \mathbf{C}_{v21} = \begin{bmatrix} -C_{s1} & C_{s1}a_1S \\ -C_{s2} & -C_{s2}a_2S \end{bmatrix}; \\
 \mathbf{C}_{v22} &= \begin{bmatrix} C_{s1} & 0 \\ 0 & C_{s2} \end{bmatrix}; \\
 \mathbf{K}_{v11} &= \begin{bmatrix} K_{s1} + K_{s2} & (-K_{s1}a_1 + K_{s2}a_2)S \\ (-K_{s1}a_1 + K_{s2}a_2)S & (K_{s1}a_1^2 + K_{s2}a_2^2)S^2 \end{bmatrix}
 \end{aligned}$$

more significant impact on accuracy than the number of training data. Furthermore, if the tolerance in ADM is set as $\epsilon = 1 \times 10^{-5}$, the proposed method can provide reasonable accuracy and reduce the calculation cost in both numerical simulations and experiment validations. If the vehicle model is known in advance and used as training data for constructing the PCA-based dictionary, the identified results will be more accurate under different noise levels and RSRs as the tolerance is set to be 1×10^{-6} .

- 4) The similarity law of VBCS is used in the laboratory experiments for constructing the PCA-based dictionary. The identified axle weights are reasonable under different vehicle models and mean velocities. However, there is still a gap between the simplified model bridge in this study and a real bridge in-situ. For a scaled bridge in laboratory in future, the experimental parameters satisfying some kind of dimensional analysis should be rigorously determined to closely match the real-world applications. Furthermore, the proposed method should be further refined to distinctly separate each axle, allowing it to handle multiple vehicle cases more effectively in the future. Besides, the training data used for constructing PCA-based dictionaries still need to be more explored.

CRediT authorship contribution statement

Bohao Xu: Writing – original draft, Validation, Software, Methodology, Investigation, Data curation, Conceptualization. **Zhilong Hou:** Validation, Methodology, Investigation, Formal analysis. **Yuhan Chen:** Validation, Methodology, Investigation, Formal analysis. **Ling Yu:** Writing – review & editing, Validation, Supervision, Resources, Project administration, Investigation, Funding acquisition, Conceptualization.

Declaration of Competing Interest

The authors declare that they have no known competing financial interests or personal relationships that could have appeared to influence the work reported in this paper.

Acknowledgments

This project was jointly supported by the National Natural Science Foundation of China under grant numbers 52178290 and 51678278.

$$\begin{aligned}\mathbf{K}_{v12} &= \begin{bmatrix} -K_{s1} & -K_{s2} \\ K_{s1}a_1S & -K_{s2}a_2S \end{bmatrix}; \mathbf{K}_{v21} = \begin{bmatrix} -K_{s1} & K_{s1}a_1S \\ -K_{s2} & -K_{s2}a_2S \end{bmatrix}; \\ \mathbf{K}_{v22} &= \begin{bmatrix} K_{s1} & 0 \\ 0 & K_{s2} \end{bmatrix}; \mathbf{M}_s = \begin{bmatrix} (m_1 + a_2m_v)g \\ (m_2 + a_1m_v)g \end{bmatrix}.\end{aligned}$$

Where, m_v and I_v are the mass and the pitch moment of inertia of vehicle body, C_{si} and K_{si} are the damping and the spring rate of i th suspensions, C_{ti} and K_{ti} are the damping and the spring rate of i th tire, S is the wheelbase and g is the gravitational acceleration [33,35,36].

Data availability

Data will be made available on request.

References

- [1] Carey C, O'Brien EJ, Malekjafarian A, Lydon M, Taylor S. Direct field measurement of the dynamic amplification in a bridge. *Mech Syst Signal Process* 2017;85:601–9. <https://doi.org/10.1016/j.ymssp.2016.08.044>.
- [2] Ni F, Zhang J, Taciroglu E. Development of a moving vehicle identification framework using structural vibration response and deep learning algorithms. *Mech Syst Signal Process* 2023;201:110667. <https://doi.org/10.1016/j.ymssp.2023.110667>.
- [3] Cao WJ, Koh CG, Smith IFC. Enhancing static-load-test identification of bridges using dynamic data. *Eng Struct* 2019;186:410–20. <https://doi.org/10.1016/j.engstruct.2019.02.041>.
- [4] Cebron D. Assessment of the dynamic wheel forces generated by heavy road vehicles[C]/Symposium on Heavy Vehicle Suspension Characteristics, 1987, Canberra, Australia. 1988.
- [5] Wang H, Nagayama T, Su D. Static and dynamic vehicle load identification with lane detection from measured bridge acceleration and inclination responses. *Struct Control Health Monit* 2021;28. <https://doi.org/10.1002/stc.2823>.
- [6] Zhou HC, Li HN, Yang DH, Yi TH. Development of moving force identification for simply supported bridges: a comprehensive review and comparison. *Int J Struct Stab Dyn* 2022;22:2230003. <https://doi.org/10.1142/S0219455422300038>.
- [7] Law SS, Chan THT, Zeng QH. Moving force identification: a time domain method. *J Sound Vib* 1997;201:1–22. <https://doi.org/10.1006/jsvi.1996.0774>.
- [8] Pinkaew T. Identification of vehicle axle loads from bridge responses using updated static component technique. *Eng Struct* 2006;28:1599–608. <https://doi.org/10.1016/j.engstruct.2006.02.012>.
- [9] Sanchez J, Benaroya H. Review of force reconstruction techniques. *J Sound Vib* 2014;333:2999–3018. <https://doi.org/10.1016/j.jsv.2014.02.025>.
- [10] Zeng Y, Feng D, Li JA, Wang B. Deep learning-based identification of vehicular moving forces for bridges without axle configurations. *Eng Struct* 2024;304:117646. <https://doi.org/10.1016/j.engstruct.2024.117646>.
- [11] Zhang C, Zhang W, Ying G, Ying L, Hu J, Chen W. A deep learning method for heavy vehicle load identification using structural dynamic response. *Comput Struct* 2024;297:107341. <https://doi.org/10.1016/j.compstruc.2024.107341>.
- [12] Yang H, Jiang J, Chen G, Zhao J. Dynamic load identification based on deep convolution neural network. *Mech Syst Signal Process* 2023;185:109757. <https://doi.org/10.1016/j.ymssp.2022.109757>.
- [13] Masanes Didyk M, Ebrahimi Zadeh Hassanabadi M, Makki Alamdar M, Eftekhari Azam S. Minimum variance unbiased Bayesian smoothing for input and state estimation of systems without direct Feedthrough: Mitigating Ill-Posedness of online load identification. *Eng Struct* 2024;298:117023. <https://doi.org/10.1016/j.engstruct.2023.117023>.
- [14] Law SS, Chan THT, Zhu QX, Zeng QH. Regularization in moving force identification. *J Eng Mech* 2001;127:136–48. [https://doi.org/10.1061/\(ASCE\)0733-9399\(2001\)127:2\(136\)](https://doi.org/10.1061/(ASCE)0733-9399(2001)127:2(136)).
- [15] Zhu XQ, Law SS. Moving loads identification through regularization. *J Eng Mech* 2002;128:989–1000. [https://doi.org/10.1061/\(ASCE\)0733-9399\(2002\)128:9\(989\)](https://doi.org/10.1061/(ASCE)0733-9399(2002)128:9(989)).
- [16] Chen Z, Chan THT, Nguyen A, Yu L. Identification of vehicle axle loads from bridge responses using preconditioned least square QR-factorization algorithm. *Mech Syst Signal Process* 2019;128:479–96. <https://doi.org/10.1016/j.ymssp.2019.03.043>.
- [17] Pan CD, Yu L, Liu HL, Chen ZP, Luo WF. Moving force identification based on redundant concatenated dictionary and weighted l1-norm regularization. *Mech Syst Signal Process* 2018;98:32–49. <https://doi.org/10.1016/j.ymssp.2017.04.032>.
- [18] Osborne MR, Presnell B, Turlach BA. On the lasso and its dual. *J Comput Graph Stat* 2020;9:319–37. <https://doi.org/10.1080/10618600.2000.10474883>.
- [19] Liu HL, Li C, Yu L, Wang YF, Zhong J. Onsite identification of moving vehicle loads on multispan continuous bridge using both dictionary expansion and sparse regularization. *J Aerosp Eng* 2021;34:04021018. [https://doi.org/10.1061/\(ASCE\)AS.1943-5525.0001258](https://doi.org/10.1061/(ASCE)AS.1943-5525.0001258).
- [20] Qiao B, Zhang X, Gao J, Liu R, Chen X. Sparse deconvolution for the large-scale ill-posed inverse problem of impact force reconstruction. *Mech Syst Signal Process* 2017;83:93–115. <https://doi.org/10.1016/j.ymssp.2016.05.046>.
- [21] Jiang J, Cui W, Chen S, Guo X, Zhao J. A novel dynamic load identification method based on improved basis functions and implicit Newmark- β for continuous system with unknown initial conditions. *Mech Syst Signal Process* 2024;208:110987. <https://doi.org/10.1016/j.ymssp.2023.110987>.
- [22] Liu HL, Yu L, Luo ZW, Pan CD. Compressed sensing for moving force identification using redundant dictionaries. *Mech Syst Signal Process* 2020;138:106535. <https://doi.org/10.1016/j.ymssp.2019.106535>.
- [23] Zhang ZH, He WY, Ren WX. Moving force identification based on learning dictionary with double sparsity. *Mech Syst Signal Process* 2022;170:108811. <https://doi.org/10.1016/j.ymssp.2022.108811>.
- [24] Xu BH, Yu L. A novel regularized adaptive matching pursuit for moving force identification using multiple criterial and prior knowledge. *Int J Struct Stab Dyn* 2023;23:2350117. <https://doi.org/10.1142/S0219455423501171>.
- [25] Qiao B, Mao Z, Liu J, Zhao Z, Chen X. Group sparse regularization for impact force identification in time domain. *J Sound Vib* 2019;445:44–63. <https://doi.org/10.1016/j.jsv.2019.01.004>.
- [26] Zhang LQ, Liang Y, Yu L. Moving force identification based on group lasso and compressed sensing. *Int J Struct Stab Dyn* 2022;22:2250170. <https://doi.org/10.1142/S021945542250170X>.
- [27] Liu J, Qiao B, Wang Y, He W, Chen X. Group sparsity extension of “Non-convex sparse regularization via convex optimization for impact force identification. *Mech Syst Signal Process* 2023;201:110661. <https://doi.org/10.1016/j.ymssp.2023.110661>.
- [28] Liang Y, Hou ZL, Yu L. An improved block orthogonal matching pursuit for moving force identification using block-sparse compressed sensing. *Mea* 2023;222:113632. <https://doi.org/10.1016/j.measurement.2023.113632>.
- [29] Yuan Y, Zhu XQ, Li J. Moving principal component analysis based structural damage detection for highway bridges in operational environments. *Sensors* 2024; 24:383. <https://doi.org/10.3390/s24020383>.
- [30] Prawin J, Rama Mohan Rao A. An online input force time history reconstruction algorithm using dynamic principal component analysis. *Mech Syst Signal Process* 2018;99:516–33. <https://doi.org/10.1016/j.ymssp.2017.06.031>.
- [31] Imani M, Ghassemian H. An overview on spectral and spatial information fusion for hyperspectral image classification: Current trends and challenges. *Inf Fusion* 2020; 59:59–83. <https://doi.org/10.1016/j.inffus.2020.01.007>.
- [32] Mohammadi MR, Fatemizadeh E, Mahoot MH. PCA-based dictionary building for accurate facial expression recognition via sparse representation. *J Vis Commun Image Represent* 2014;25:1082–92. <https://doi.org/10.1016/j.jvcir.2014.03.006>.
- [33] Law SS, Bu JQ, Zhu XQ, Chan SL. Vehicle axle loads identification using finite element method. *Eng Struct* 2004;26:1143–53. <https://doi.org/10.1016/j.engstruct.2004.03.017>.
- [34] Wu SQ, Law SS. Vehicle axle load identification on bridge deck with irregular road surface profile. *Eng Struct* 2011;33:591–601. <https://doi.org/10.1016/j.engstruct.2010.11.017>.
- [35] Wang H, Nagayama T, Su D. Estimation of dynamic tire force by measurement of vehicle body responses with numerical and experimental validation. *Mech Syst Signal Process* 2019;123:369–85. <https://doi.org/10.1016/j.ymssp.2019.01.017>.
- [36] Feng D, Sun H, Feng MQ. Simultaneous identification of bridge structural parameters and vehicle loads. *Comput Struct* 2015;157:76–88. <https://doi.org/10.1016/j.compstruc.2015.05.017>.
- [37] ISO. No. 8608. Mechanical vibration-Road surface profiles-Reporting of measured data, Standard, 2016. Geneva, Switzerland: ISO; 2016.
- [38] Asnachinda P, Pinkaew T, Laman JA. Multiple vehicle axle load identification from continuous bridge bending moment response. *Eng Struct* 2008;30:2800–17. <https://doi.org/10.1016/j.engstruct.2008.02.018>.
- [39] Zhang J. Optimal implicit single-step time integration methods with equivalence to the second-order-type linear multistep methods for structural dynamics: accuracy analysis based on an analytical framework. *Comput Methods Appl Mech Eng* 2024; 418:116503. <https://doi.org/10.1016/j.cma.2023.116503>.
- [40] Yu L, Chan THT. Recent research on identification of moving loads on bridges. *J Sound Vib* 2007;305:3–21. <https://doi.org/10.1016/j.jsv.2007.03.057>.
- [41] Zhou HC, Li HN, Yang DH, Yi TH. Moving force identification of simply supported bridges through the integral time domain method. *J Sound Vib* 2022;534:117046. <https://doi.org/10.1016/j.jsv.2022.117046>.
- [42] Qiao B, Zhang X, Wang C, Zhang H, Chen X. Sparse regularization for force identification using dictionaries. *J Sound Vib* 2016;368:71–86. <https://doi.org/10.1016/j.jsv.2016.01.030>.
- [43] Jolliffe IT, Cadima J. Principal component analysis: a review and recent developments. *Philos Trans R Soc Math Phys Eng Sci* 2016;374:20150202. <https://doi.org/10.1098/rsta.2015.0202>.
- [44] Mahi A, Gao R. PCA-based feature selection scheme for machine defect classification. *Instrum Meas IEEE Trans* 2005;53:1517–25. <https://doi.org/10.1109/TIM.2004.834070>.
- [45] Yu GS, Sapiro G, Mallat S. Solving inverse problems with piecewise linear estimators: from Gaussian mixture models to structured sparsity. *IEEE Trans Image Process* 2012;21:2481–99. <https://doi.org/10.1109/TIP.2011.2176743>.

- [46] Xie D, Singh SB, Fluder EM, Schlick T. Principal component analysis combined with truncated-Newton minimization for dimensionality reduction of chemical databases. *Math Program* 2003;95:161–85. <https://doi.org/10.1007/s10107-002-0345-7>.
- [47] Nie Z, Shen Z, Li J, Hao H, Lin Y, Ma H, et al. Using a single sensor for bridge condition monitoring via moving embedded principal component analysis. *Struct Health Monit* 2021;20:3123–49. <https://doi.org/10.1177/1475921720980516>.
- [48] Luo ZW, Yu L. Regularization strategies for contiguous and noncontiguous damage detection of structures. *Int J Comput Methods* 2021;18:2140001. <https://doi.org/10.1142/S0219876221400016>.
- [49] Yuan M, Lin Y. Model selection and estimation in regression with grouped variables. *J R Stat Soc Ser B Stat Methodol* 2006;68:49–67. <https://doi.org/10.1111/j.1467-9868.2005.00532.x>.
- [50] Deng W, Yin W, Zhang Y. Group sparse optimization by alternating direction method. *Wavelet Sparsity XV* 2013;8858:242–56. <https://doi.org/10.1117/12.2024410>.
- [51] Wright SJ, Nowak RD. Sparse reconstruction by separable approximation. *IEEE Trans Signal Process* 2009;57:2479–93. <https://doi.org/10.1109/TSP.2009.2016892>.
- [52] Tang X, Feng G, Cai J. Weighted group sparse representation for undersampled face recognition. *Neurocomputing* 2014;145:402–15. <https://doi.org/10.1016/j.neucom.2014.05.012>.
- [53] Wang Y, Li X, Ruiz R. Weighted general group lasso for gene selection in cancer classification. *IEEE Trans Cybern* 2019;49:2860–73. <https://doi.org/10.1109/TCYB.2018.2829811>.
- [54] Hirose K, Konishi S. Variable selection via the weighted group lasso for factor analysis models. *Can J Stat* 2012;40:345–61. <https://doi.org/10.1002/cjs.11129>.
- [55] Li J-A, Feng D. Fatigue life evaluation of bridge stay cables subject to monitoring traffic and considering road roughness. *Eng Struct* 2023;293:116572. <https://doi.org/10.1016/j.engstruct.2023.116572>.
- [56] Majdoub KE, Giri F, Chaoui FZ. Adaptive backstepping control design for semi-active suspension of half-vehicle with magnetorheological damper. *IEEECAA J Autom Sin* 2021;8:582–96. <https://doi.org/10.1109/JAS.2020.1003521>.
- [57] Pinkaew T. Identification of vehicle axle loads from bridge responses using updated static component technique. *Eng Struct* 2006;28:1599–608. <https://doi.org/10.1016/j.engstruct.2006.02.012>.
- [58] Xu B, Chen YH, Yu L. Identification of moving vehicle loads using instantaneous vision-based vehicle spatiotemporal information and improved time domain method. *Int J Struct Stab Dyn* 2023;2450163. <https://doi.org/10.1142/S0219455424501633>.
- [59] Gui S, Chao Z, Chen S. Similarity law of scale-model test system for vehicle-bridge coupling vibration. *J Chongqing Jiaotong Univ(Nat Sci)* 2015;34:10–4. (<http://xbzk.cqjtu.edu.cn/CN/10.3969/j.issn.1674-0696.2015.02.03>).
- [60] Hou ZL, Liang Y, Yu L. A novel semi-convex function for simultaneous identification of moving vehicle loads and bridge damage. *Mech Syst Signal Process* 2025;223:111900. <https://doi.org/10.1016/j.ymssp.2024.111900>.